Strål
säkerhets
myndigheten

Research

Fibre Clogging in Nuclear Power Plants

An Investigative Study on the Filter Mat Forming and
Retention of Fibres on Screens of Various Design.

2020:07

Authors: Jakob D. Redlinger-Pohn, Michael Liverts,
and Fredrik Lundell. Department of Mechanics,
KTH The Royal Institute of Technology

SSM perspective

Background

Emergency core cooling systems in boiling- and pressurized water reactors use strainers. Their purpose is to filter out foreign material suspended in the cooling water so this material does not reach the reactor. After the 1992 event at Barsebäck nuclear power plant when the strainers of the emergency cooling system was clogged due to fibers in the cooling water, all Swedish nuclear plant increased the surface size of the strainers, to avoid them from being clogged. The risk of accumulation on the strainers is increased pressure drop over strainers, potentially causing cavitation in the emergency cooling pumps and an excessively reduced flowrate. An increase in the surface size of the strainers has the side effect of more fibers passing through the strainers. If the foreign material pass through the strainers, they lose their purpose of reducing the risk of clogging the reactor, which can affect the removal of the residual heat. Examples of foreign materials are debris, chemical compounds, and fibres. In the event of Loss of Coolant Accident caused by a pipe break, insulating material consisting of fibres, if present in the containment, is likely to tear off. In boiling water reactors, the fibres can mix with the water in the condensation pool, and in pressurized water reactors, the fibres can reach the sump. In either case, the fibres mix with the emergency cooling water. Additional loose debris may mix into the water. pH-regulating chemicals, with the purpose of binding the iodine, may form sticky chemical compounds. The foreign material can either remain in the pool or sump, accumulate on the strainer surfaces, or pass through it.

There is further background on the subject under the U.S. Nuclear Regulatory Commission (NRC) Generic Safety Issue (GSI) -191, "Assessment of Debris Accumulation on Pressurized-Water Reactor Sump Performance".

Results

The experiment in this study investigates different strainer surface geometries for different sizes of holes and orifice separation. In addition, different size meshes are investigated to see their effectiveness in retaining fibers.

Fibre formation on strainers depends on the fibre length L_{Fibre} with respect to the screen opening (hole) D_{Open}, and screen hole spacing (solid) S_{Open}. We focused on the deposition of fibres on the screens classified by their geometry in relation to the fibre length and identified 4 regimes based on L_{Fibre}/D_{Open}, and L_{Fibre}/S_{Open}. Most effective was the retention of fibres in regime I. Surprisingly, also screens in regime II, which hole size D_{Open} is larger than the fibre length L_{Fibre} got covered. The coverage rate was sensitive on the hole spacing S_{Open}. Findings per regime is summarized as:
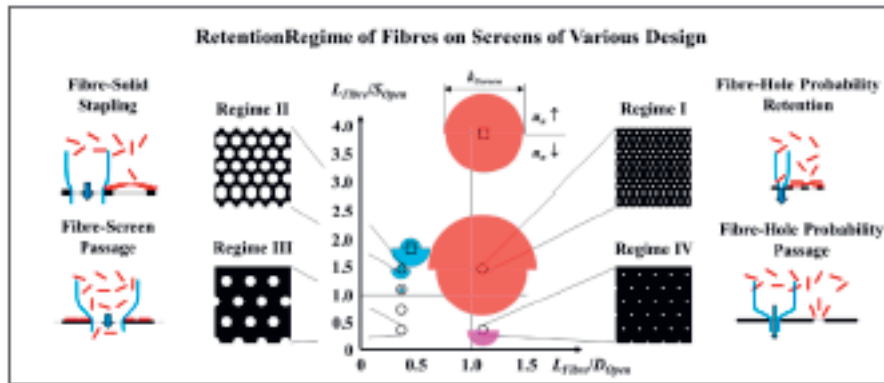
Regime I, small holes and small spacing, retained fibres that were longer than the diameter or width of the holes. Fibres bridge the openings with their length.

Regime II, large holes and small spacing, was found collecting fibres on the solid hole spacing which then covered the screen with time. The regime was classified as fibre-solid stapling.

Regime III, large holes and large spacing, extends fibre stapling from regime II to cases where the flow obstruction, i.e. S_{Open}, was large compared to the fibre length L_{Fibre}. The solid part of the screen was covered, but the holes remained open. Further increase in S_{Open} prevented significant stapling of fibres on the screen. An increase of fibre concentration led to the formation of a fibre mat at low approach velocity. The regime was classified as fibre-screen passage. Fibre mat formation in regime III was followed up seeding with a fraction of longer fibres, which result in regime I retention on the screen. For low approach velocity u_n, an addition of ca. 1% of the longer fibres which bridged the holes, was enough to retain the smaller fibres on the screen.

Regime IV, small holes and large spacing, was found sensitive to the approach velocity. The screen geometry results to a small open area A_{Open}, which was 6% for the studied case. For low approach velocity u_n a nearly, but not full, screen coverage was recorded. Fibres were bridging the openings.

Initial covered holes were found unplugging. Higher approach velocity prevented fibre deposition on the screen.

Fibre mat formation on fuel assembly followed the fibre mat formation on screens. Conclusions on the fibre mat formation from this study were thus direct applicable to fibre mat formation on fuel assemblies. In particular we showed for PLUS7 protective grid a fibre stapling process leading to the coverage with a fibre mat. We suggest including the parameters L_{Fibre}/D_{Open}, and L_{Fibre}/S_{Open} into design consideration of fuel assemblies.

Relevance
SSM initiated this project in order to increase the understanding of which parameters are important for the accumulation of the fibres on the strainers and if it can be improved. It is desirable that a minimum amount of fibres pass through the strainers since they can cause downstream effects and potentially hamper the emergency core cooling system, the containment spray system, and decrease the heat-transfer in the reactor. The investigation is relevant for the strainers and the fuel assemblies in boiling water reactors and pressurized water reactors.

Need for further research
Extending the current set of experiments to include various fibre lengths and fibre length distributions would be valuable. A number of spacers and protected grid layers were printed but never tested. The screen performs poorly under certain conditions. In one of the experiments, many fibres passed though the strainer holes when their diameter was small compared with the spacing between them. The fibre orientation under different conditions might play a role. Since the holes are small in relation to the screen surface, the flow will go parallel with the surface, and into the holes. The acceleration of the flow might be higher for small holes compared with larger holes. This entrainment effect can potentially explain why the fibres cannot cling to the screen surface, and will instead pass through the strainer holes. Future research can test these hypotheses.

Fibre deposition in compact heat exchangers could also be an area of future research. In most Swedish boiling water reactors, the system for containment spraying include strainers and compact heat exchangers, which cool the spray water. The containment spraying system takes water from the same source as the emergency cooling system, and can experience similar downstream effects.

Project information
Contact person SSM: Peter Hedberg
Reference: SSM2017-4551 / 7030198-00

Strål säkerhets myndigheten

Swedish Radiation Safety Authority

Authors: Jakob D. Redlinger-Pohn, Michael Liverts, and Fredrik Lundell
             Department of Mechanics, KTH The Royal Institute of Technology

2020:07

Fibre Clogging in Nuclear Power Plants

An Investigative Study on the Filter Mat Forming and Retention of Fibres on Screens of Various Design

This report concerns a study which has been conducted for the Swedish Radiation Safety Authority, SSM. The conclusions and view-points presented in the report are those of the author/authors and do not necessarily coincide with those of the SSM.

A report on

Fibre Clogging in Nuclear Power Plants

An Investigative Study on the Filter Mat Forming and Retention of Fibres on Screens of Various Design

Jakob D. Redlinger-Pohn[*], Michael Liverts, and Fredrik Lundell

Department of Mechanics, KTH The Royal Institute of Technology

Teknikringen 8, 10044 Stockholm, Sweden

*Corresponding author: E-mail: edu.redlinger@gmail.com; Tel.: +46 8 790 7625

Abstract

Crucial in the safe operation of Nuclear Power Plants is the guaranteed cooling of the nuclear fuel, also in emergency cases and during incidents. An identified risk to the reactor core cooling is the collection of fibres on screens and strainers, formation of fibre mats and the consequent filtration. Solutions to this issue following first incidents included increasing in screen surface area and modelling of the pressure loss for differing mixtures of fibres and particles. The retention of fibres on the screen and the formation of a fibre mat which precedes any particle filtration was however neglected and is yet not understood. Also, the potential leakage of fibres to the fuel assembly before a mat is formed can be critical.

In this report we follow-up fibre accumulation in paper production. Such is known to either result from *probability retention*, i.e. the fixation of a fibre on openings that are smaller than the fibre length, or *stapling*, i.e. the fixation of a fibre as a result from fibre-solid friction being larger than hydrodynamic drag forces on the fibre. This study expands the knowledge of fibre mat formation from retention on screens of small hole size and small hole spacing to general cases. We manufactured and studied screens that were defined by their geometry in comparison to the fibre length, i.e. fibre length to hole size, and fibre length to hole spacing. Screen coverage for cases of small hole size followed fibre probability retention. Deposition probability depends on the fibre orientation and is independent on the fibre concentration for dilute suspensions. Fibre deposition was decreased for screen open area *smaller* than 10%. Surprisingly, screen coverage was also achieved for screens with holes larger than the fibre length since fibres stapled on the areas in between the holes. Screen coverage from stapling is efficient but slower than from retention. An increase in the hole spacing decreased the chance of fibre-screen friction-based retention and the screen remained open and clean.

The suspension volume that led to the formation of the fibre mat on screens by probability retention was found to be independent on the approach velocity. Fibre mat formation from stapling, however, was dependent on the approach velocity and was lower for increased velocity. From the screen coverage rate, we could show that the increase in the screen surface area, the typical reaction to past incidents, increased the fibre suspension volume passing through the screen before a totally filtering fibre mat is formed. Hence, more fibres bypassed the screen. A combination of an inefficient screen followed by a more efficient screen downstream improved fibre retention, but the fibre mat formed between the screens persisted screen cleaning by back-flushing.

Fibres passing the screen will enter the nuclear reactor chamber with the coolant. Literature notes the formation of a particle filtering fibre mat on the protective grid of the fuel assembly. We reproduced the protective grid to detail on the deposition mechanism which we found equivalent to fibre-screen deposition. For the studied PLUS7 protective grid layer we noted the chance of fibre stapling, i.e. hole spacing is smaller than the hole opening.

Contents

1. Introduction

The risk of nuclear energy rose in the general awareness latest after the Fukushima Daiichi accident. In Europe, policymakers reacted by re-evaluating their national energy production strategies [1]. The European Commission does note nuclear energy as a means to decarbonize energy production in its *Energy Roadmap 2050* but sees a decrease of nuclear energy until 2030 based on its 2005 share [2]. Predictions for 2050 range from substantial decrease to an increase, which expresses uncertainty on the European nuclear strategy. The forecast given by the International Atomic Energy Agency (IAEA) predicts a fast to slow decline in nuclear energy in Europe based on its 2017 share [3]. Scenarios for the lower decline, with nuclear power maintaining its share in the European energy market, necessitate a prolonged operation of current nuclear power plants outside of their design life [3,4]. In order to accomplish the regulatory bodies requirements, it is mandatory to review all the potential issues associated with the operation of systems of a reactor for such long periods of time [5,6].

One risk in the operation of a nuclear power plant (NPP) is a drop in the reactor coolant flow rate resulting from increased pressure drop over strainers (boiling water reactor, BWR) and screens (pressurized water reactor, PWR) that are clogged by fibres. The fibres are present in small quantity and origin from unspecific sources, i.e. latent fibres, or are created in larger quantity during a Loss of Coolant Accident (LOCA) that involves pipe breakage and/or malfunctioning valves. The suspended fibres were found to form a mat, which then filtered suspended particles that otherwise pass the strainers and screens. This led to a recorded drop in coolant flow rate [7–9]. Whilst this formation of a fibre mat that retains particles was a surprise to the operators at the first incidents, it is nothing unexpected from a fibre suspension perspective. It is the business foundation of paper production enterprises.

A resolution to the unexpected reduction in coolant flow rate over the Emergency Core Cooling System (ECCS) strainer was, (i) an increase of the screen surface area [10] and (ii) the attempt to predict pressure losses for NPP LOCA scenarios [9,11,12]. However, none of the previous studies investigated the initial fibre retention that precedes any particle filtration from the suspension. Clearly, this initial fibre retention is key to understand clogging of screens and strainers in any operation. Furthermore, fibres passing the screens and strainers might cause problems in the reactor core. Thus, it is also necessary to control the amount of fibres passing the screens and strainers before a fibre mat is formed.

With the safety of the aging fleet of European nuclear power plants in mind we asses in this report the regimes of fibre mat forming on typical ECCS BWR strainer (mostly hole plates), and PWR screens (mostly wire meshes).

In chapter 2 we establish a broader understanding of the problem putting a papermaker's view on the nuclear industry's problem. Specifically, we review the literature on forming of fibre mats from the paper industry, and general particle filtration, as well as nuclear industry-specific filtration studies. The conclusions from the literature study framed the design of the experimental study.

In chapter 3 we describe our approach and the experimental method. Sets of screens were designed and produced for an optical investigation of the screen coverage by restrained

fibres. Screen coverage was tracked by comparing RGB (red, green, blue) colour values of the model fibre to the clean screen and evaluated by appropriate thresholding.

In chapter 4 we present the results and the insights gained. We first present details on the screen coverage for a monodisperse fibre suspension on screens that fall in different regimes. In a set of experiments that follow the regime analysis, we demonstrate the impact of fibre concentration and polydispersity on the fibre retention on screens and discuss the impact of the accelerating flow upon screen passage on the fibre orientation and hence the chance of deposition.

In chapter 5 we discuss the screen performance considering an increase in screen surface area and application of succeeding screens based on our insights and results from the detailed study in chapter 4.

In chapter 6 we expand the fibre deposition towards fibre mat forming on fuel assemblies. The first layer of a protective grid can be regarded as a screen and thus, fibre deposition follows the principles identified in chapter 4.

In chapter 7 we conclude this study summarizing the key findings. The findings are put into a larger context and remaining open questions are discussed.

Appendix A discusses the expected fibre networking regime in nuclear power plant pool and sump based on accessible literature. Appendix B discusses the fibre deposition on fuel assemblies and reviews the design of protective grids. The design of PLUS7 protective grid is well documented in the literature and its geometry has been extracted for reproduction as part of this study.

2. Fibre Retention and Particle Filtration

Filtration can be seen either as removal of particles from a suspension, or the clarification of a suspension from particles. The viewpoint is decided by whether the liquid or the particles are regarded as the valuable part, or the product. For example, a reactor core coolant should be clear from debris. Typically, classification differentiates whether suspended particles deposit on, or in a filter and if the process can be operated continuous or discontinuous (for examples needs to be stopped with the pressure loss over the filter cake exceeding available pump head). D.B. Purchas and K. Sutherland in their *Handbook of Filter Media* refine the filtration process characterization into [13]:

(i)   Surface straining. Particles that are larger than the opening of the filter deposit on the surface. That is the main mechanism for screens, filter cloths, but also membranes.

(ii)   Depth straining. Filter media that are thick with respect to the opening size can retain particles in the filtration direction. Especially for cases of varying opening size, i.e. pore diameter. Particles are then stuck in the pore. Associated with non-woven filter media, for example, thick fibre mats.

(iii)   Depth filtration. Particles smaller than the opening size or pore size of a comparable thick filter can be retained by adherence to the filter material upon contact. An example is air filters.

(iv)   Cake filtration. Suspended particles filtered, or strained by a screen, filtration cloth, or filter mat build a cake which in turn acts as a filter to the approaching suspension. Suspended particles can either be retained by the cake, i.e. surface straining where the opening size is now the cake pore size or straining if particles are small enough to enter the cakes pore. Particles that initially would pass the screen are then retained by the formed filtration cake.

Obviously, not one of the processes listed above is responsible alone for the particle removal from a suspension, but a combination of those. An example is the filtration of fibres and particles on the Emergency Core Cooling System (ECCS) strainer and screen where (i) first fibres are retained on the screen, (ii) filtration cloth is formed (or mat for higher thickness), which (iii) then filters fibres and particles from the approaching suspension. A schematic illustration is given in Figure 1.

A special note shall be given on the nature of fibres and the used terminology of retention, rather than filtration or straining. Although fibres are particulates as well, particles are often associated with a more spherical shape. Fibres may then be described by their key characteristic as elongated, non-spherical particles. It is this elongation, represented by the fibre aspect ratio AR, i.e. the fibre length L_{Fibre} compared to the fibre diameter D_{Fibre} ($AR = L_{Fibre}/D_{Fibre}$), that gives a large interaction distance to fibres. As a result, fibres with D_{Fibre} of μm, but L_{Fibre} of mm, easily form networks at low concentration, and bridge openings, such as screen holes. Another consequence from elongation is an increase in fibre flexibility. Discussed in detail later, the retention of fibres on a screen is then a probabilistic filtration process depending on the fibre orientation with respect to the fibre length and screen opening size.

Filtration of Particulates at Loss of Coolant Accident (LOCA)

The presence of fibres in the NPP and their accumulation on strainers came into awareness in the 1990s by a series of incidents at boiling water reactors (BWR). These events and the development of understanding are summarized in a chronological review by Gordon H. Hart [7]. Initially, BWR strainers were designed under the assumption of partial strainer coverage, to filter debris that otherwise may damage the emergency core cooling system ECCS [11], but not for filtration operation withstanding pressure difference over the strainer. Suppression pools in BWR and sumps in pressurized water reactor (PWR) were generally assumed clean. That view changed when a series of issues in BWRs revealed the presence of latent fibres (including fibres from air filters, and other unspecified sources [14]), and particles (including rust from carbon tubing, concrete dust, and paint). Those fibres were retained by the strainer and formed a filtration cloth which subsequent filtered the particles from the suspension. A resolution to these issues was the increase of the screen surface area by the BWR operators. Hence, the area-specific pressure drop decreased [7,10]. In addition, the U.S. Nuclear Regulation Commission (NRC) issued and contracted research, first on BWR suppression pool strainer clogging at Alden Research Laboratory [11,12], and then on PWR screen blockage at Los Alamos National Laboratory [9]. These studies focused on describing and quantifying (i) the disintegration of the insulation material, i.e. NUKON® glass fibres, into fibre bundles and fibres, (ii) the transport to the strainer, and (iii) its filtration. The aim was on the description of expected pressure loss and reduction of the coolant flow for accident scenarios. A significant finding is that only a small amount of fibres is needed to generate a large pressure drop. That is mentioned by Hart [7] as *thin mat effect*. A large pressure drop results from the filtered particles. The contribution of the fibres is to form a filtering fibre mat.
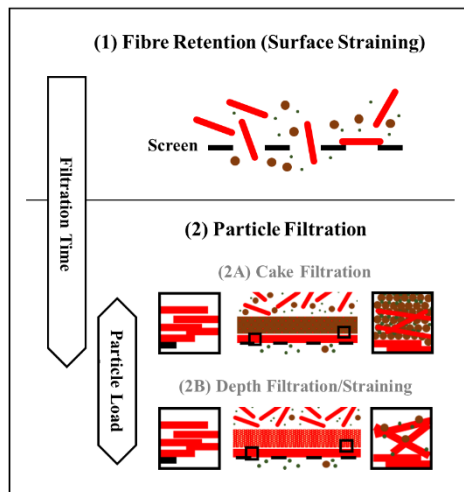
Figure 1: Time evolution of the fibre retention and particle filtration process. (1) First fibres (in red) are retained forming a mat. (2) Particles (in brown) are then filtered by the mat. The sub-regime depends on the volume-ratio of particles to fibres.

Due to the operational importance of the coolant flow, the intention of previous studies was to predict and model the pressure loss on the strainer, or screen for the design of the ECCS system. The studies in their methodology mimic the diversity in ECCS strainer and screen design found for differing types of NPP. Hence, the experimental methods differ and

change with time. For example, previous studies neglect the pairing of fibre length and screen dimension that we will find critical.

Fibre suspensions were mostly prepared from NUKON® insulation material (glass fibres with a diameter of ca. 7 μm (PCI Performance Contracting, Inc., USA). NUKON® glass fibre mat is used for insulation in BWR in the 1990s [11] and afterward. But also, experimental work for heat shielded, low fibre PWR were made with NUKON® fibre slurry as a surrogate for any latent fibres [15,16]. The preparation procedure aims to mimic the transport and destruction of NUKON® insulation during LOCA including (i) initial heat treatment to emulate aging followed by (ii) cutting, and (iii) dry dispersion in a blender (known as the WCAP method [17]), or wet dispersion (known as NEI method [18]). The modified NEI method skips the cutting but delaminates the mat in more layers before wet dispersion [19,20].

Fibrous debris was classified in groups by their measured sedimentation velocity and described by their appearance. These aspects were important in the first investigations studying the transport of the fibres to the strainer [11,20]. The debris size classification is summarized in Table 1 including a comparison of the results from different preparation methods from Ali, and Badford [19], and Williams [20]. They report that experiments aiming to quantify the chemical head loss (precipitated particles) note a higher sensitivity of the pressure loss for WCAP prepared fibres whereas the NEI method results had a higher degree of reproducibility. Clearly, experimental results in the previous literature need to be interpreted with respect to the preparation method.

Suh [15], and Suh et al. [16] measured the fibre length distribution of samples prepared according to the APR1400 method (a variation of the NEI method) and the WCAP method (WCAP-16793). The results are discussed in detail in Appendix A. The WCAP prepared fibres were shorter and had a larger proportion of fragments smaller than 0.5 mm. Unfortunately, they failed to report the basis of the length distribution (i.e. number based, or length based), which makes the interpretation of their data difficult. Key values L_1, which is the length-based mean-fibre length, and x_{90} which represent the fibre length exceeded by 10%, are given for two assumptions of the distribution basis in Table 2.

Suh [15] performed a by-pass test on an ESSC strainer (Transco Products Inc., IL, USA) with a hole size of 2.38 mm. The spacing was not reported, but images show a spacing smaller than the hole size. Arguably, the larger fibre, which length is slightly below the hole size, is, however, larger than the hole spacing. Reported images present partly covered ECCS screen and state a fibre by-pass of 25% (retention of 75%). By-passing fibres were then found retained at the nuclear fuel assemblies and filtering particles there. As a result, the pressure loss over the fuel assembly increased.

The strainers used in the studies where comparable, but the exact choice seems somewhat arbitrary. A larger proportion of experiments was performed in filtration columns, i.e. pipe with a screening section in either the vertical or the horizontal orientation. An overview of test conditions in the literature is given in Appendix A. The suspension approach direction on the screen is typically normal; a clear idealization compared to the real NPP flow cases. Rao et al. [9] note on the comparability of BWR strainer clogging to PWR screen clogging, that strainers are mostly hole plates, i.e. perforated plates, and screens are wire meshes with a typical mesh size of 3.175 mm. Other reported strainer and screen dimensions have an opening size between ca. 2.5 mm and 3.5 mm and spacing in the same order or smaller.

Table 1: Classification of fibrous debris by their sedimentation velocity and appearance [11]. Model suspension per preparation method is indicated [19,20].

		Description	Filtration Efficiency	Preparation Method		
1		Very small pieces of glass fibre that appear cylindrical of varying *AR*. Settling velocity: 0.1 mm/s – 3.5 mm/s	Un-known	WCAP		
2		Single flexible strand of glass fibre. Settling velocity: 0.1 mm/s – 3.5 mm/s	Appr. 1.0			Mod. NEI
3		Multiple attached of interwoven strands of glass fibre. Settling velocity: 0.1 mm/s – 10 mm/s	1.0			
4		Formation of fibres into clusters. Settling velocity: 0.1 mm/s – 10 mm/s	1.0		NEI	
5		Clumps of fibrous debris. Settling velocity: 0.1 mm/s – 10 mm/s	1.0			
6		Large clumps of fibres. Settling velocity: 0.1 mm/s – 10 mm/s	1.0			
7		Pre-cut pieces of the insulation material. Settling velocity: 0.1 mm/s – 10 mm/s	1.0			

Table 2: Key values of the fibre length distribution from Suh [15,16]. Fibre length distribution results are discussed in Appendix A.

	Basis in Suh: Length [mm]		Basis in Suh: Number [mm]	
Method	APR1400	WCAP-16793	APR1400	WCAP-16793
L_1	0.73	0.57	1.25	1.02
x_{90}	1.56	1.16	2.34	2.13

A third aspect, in addition to the combination of fibre length and strainer/screen dimension that will be found to be important is the approach velocity. In the case of a pump power large enough to balance the pressure loss, the approach velocity results from the (i) needed reactor coolant flow and (ii) filter surface area. The filter surface area is, however, a design aspect that needs to take the expected debris quantity and resulting increase of pressure loss

in consideration. The impact of the approach velocity is discussed in the literature in terms of pressure loss, but not with respect to the fibre retention and fibre mat forming.

The summary above is the general impression from the survey of published literature on fibre retention and filtration phenomena on BWR strainers and PWR screens. Although fibre mat forming is addressed by the NRC in the Generic Letter GL 2004-02 the issue is yet not concluded. As a perspective and broader basis for the experimental investigation, a review of the literature on the formation and stapling of fibres in the cellulose processing follows.

Forming of Fibre Mat on Meshes in Paper Production

Research on the retention and passage of fibres through a screen, which typically is a wire mesh in paper manufacturing and cellulose pulp processing, has a long tradition. Examples are the forming of a paper sheet from a thin fibre suspensions [21], or length classification of fibre suspensions [22–25]. Sheet forming describes the thickening and dewatering of a suspension of cellulose fibres, which may also contain organic and inorganic fines material (e.g. calcium carbonate particles). J.D. Parker summarized the fundamentals of fibre retention and forming [21]. In a dilute suspension of pulp fibres, the inertial forces on individual fibres are small, why the fibres closely follow the flow of the fluid. However, for networked fibres at higher concentration or in fibre flocs, the motion of an individual fibre is restricted. The forming process is a dynamical process controlled by several interdependent, concomitant effects. The most important considerations that are also of interest for the fibre retention process in NPP will be reviewed in the following.

Fibre Suspension Filtration or Fibre Suspension Thickening

The fibre mat structure defines the quality of the formed paper, for example strength, and results directly from the water removal process. An excellent introduction is given in the paper of Radvan, and Dodson [26], and the review by J.D. Parker [21].

Fibre suspension filtration is the retention of fibres from a dilute suspension resulting into a layered structure of the fibre mat, i.e. fibres are deposited on a 2D plane. Improved uniformity of the fibre mat thickness is achieved by dilution, i.e. lower fibre concentration. At lower concentrations, the suspension self-adjusts to differences in the pressure drop resulting from uneven mat thickness: the pressure drop is lower at regions of fewer deposited fibres and hence, the flow is directed there leading to a locally increased fibre deposition. This is referred to as the self-healing effect [27]. The concentration of non-fibrous particles is typically higher at locations of increased flow rate (i.e. locally and momentarily thinner fibre mat) [28,29].

Fibre suspension thickening, also termed consolidation, is the removal of fluid from a suspension of interacting, or networked fibres. In this case, the fibre mat has a felted structure, i.e. it has a 3D structure retaining random fibre orientation from the networked fibres. Thus, the inner structure of the fibre mat formed on a screen depends on the level of fibre interaction in the suspension and whether fibres were flocculated or not.

The chance of fibre-fibre interaction and the degree of flocculation depends on the volume concentration $C_{v,Fibre}$, i.e. the number of fibres present in a given volume, and the fibre aspect ratio AR. The degree of fibre interaction and thereby fibre flocculation (the tendency of fibres to form tufts of fibres interlocking each other) is typically quantified by the crowding number N_{CW} which compares the expected average number of fibres within the volume defined by a sphere of diameter equal to the fibre length L_{Fibre} [30,31]:

$$N_{CW} = \frac{2}{3}\left(\frac{L_{Fibre}}{D_{Fibre}}\right)^2 C_{v,Fibre} = \frac{2}{3}AR^2 C_{v,Fibre}. \tag{1}$$

The crowding number N_{CW} has been found to characterize different regimes of fibre interaction and connectivity. Those regimes are discussed with respect to LOCA conditions in Appendix A. From the limited data set available, we conclude that a free, and dilute fibre flow is to be expected in NPP. Thus, the fibres can be regarded to be individually suspended and fibre filtration resulting in a 2D plane fibre sheet on the screen is to be expected.

Retention of Fibres from Thin Suspension

As mentioned earlier, the initial retention of fibres on wire mesh is a probabilistic process, depending on the fibre orientation, the fibre length L_{Fibre}, and size of the openings in the screen D_{Open}, as sketched in Figure 2a. Two fibres (a red and a blue), with $L_{Fibre} > D_{Open}$, approach the screen at two different inclinations with respect to the flow direction (in the x-direction). Assuming an axisymmetric flow, the orientation can be described by ϕ which denotes the deviation of the fibre axis from the screen normal. For a small angle (the blue fibre), the fibre length projected on the screen (blue dashed line) is smaller than D_{Open} and the fibre passes through the opening. For a high deviation from the flow direction (the red fibre), the projected length on the screen $L_{Projected}$ is larger than D_{Open}, and the fibre will be retained on the screen. Consequently, from the fibre deposition, the extent of the open area is then reduced, increasing the chance of fibre retention for following fibres. Estridge [32], and Abrahms [33] discuss the retention probability for the pairing of L_{Fibre} to D_{Open} (Figure 2b). The fibre retention probability is derived from geometrical considerations and validated against experimental results with rectangular and parallel wire meshes. The effect of hydrodynamic drag on the fibre was neglected in these theoretical assumptions. High initial retention of fibres on square wire meshes is achieved when fibres are larger than 2.5 times the opening size. However, also fibres smaller than the opening size can be retained. That is for cases when the fibre bridges two corners of the square mesh. The theory matches nicely the data of fibre screen passage probability from Andersson & Bartok [25]. They evaluated the fibre passage in a Bauer-McNett (BMC) classier, i.e. a cascade of four 28 mesh screens with a feedback loop. Once a steady state was reached, the fibre concentration in the circulating fluid can be used to determine the passage probability. Although not explicitly shown here, the retention of fibres by circular holes, for example, staggered hole plates, is of comparable nature.
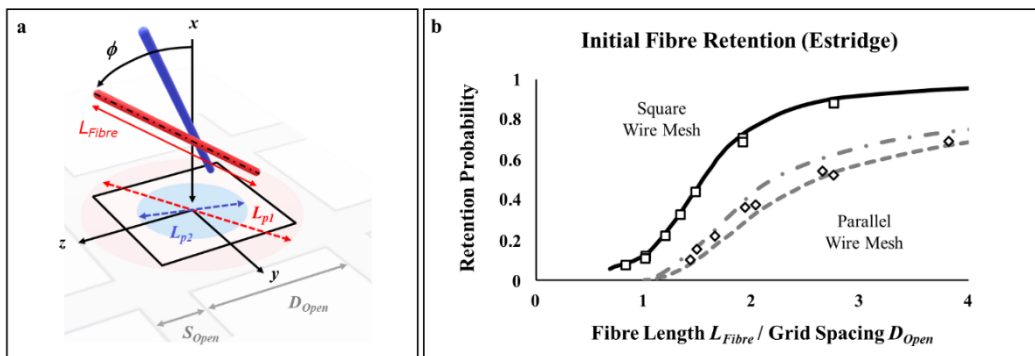
Figure 2: Fibre retention on wire meshes. a: schematic of two fibres approaching a screen with square openings at different orientations. The red fibre is retained on the screen, and the blue fibre is accepted through the screen. b: Initial fibre retention dependence on L_{Fibre}/D_{Open} for square wire meshes and parallel wire meshes as given by Estridge [33],.

The orientation of the fibre is however not static, but dynamic and can evolve with the suspension flow. For flows past screens, the fluid has to pass through the openings and

accelerate from the bulk velocity u_n to the hole velocity u_{Hole}, which depends on the screen open area A_{Open}: $A_{Open}u_{Hole} = u_n$. This results in an extensional flow upstream of the screen. As a result, the fibre rotates in the flow field and its orientation is time-dependent. An analytical solution for the fibre rotational motion in flow gradients was first presented by Jeffery [34]. A detailed introduction to the current state of understanding of dilute fibre suspension flows, amongst other sources, may be found in research work from Lundell, and Söderberg group [35–38]. For extensional, or accelerating flow situations Håkansson et al. reviews and reports the solution of Jeffery's equation for the rotational velocity $\dot{\phi}$ as [39]:

$$\dot{\phi} = \frac{\partial \phi}{\partial t*} = \frac{\partial u*}{\partial x*}\left(\frac{1-AR^{-2}}{1+AR^{-2}}\right)\frac{3}{2}\cos(\phi)\sin(\phi) \tag{2}$$

where $u*$ is the fluid velocity normal to the screen and $\partial u*/\partial x*$ the acceleration. The change in the fibre orientation distribution ψ along a normal to the screen that goes through the centre of a hole is described by a modified Smoluchowski equation. If only the convective term is considered, and rigid and inertialess fibres are assumed the resulting equation is:

$$u*\frac{\partial \psi}{\partial x*} = -\frac{1}{\sin(\phi)}\frac{\partial}{\partial \phi}\left(\sin(\phi)\dot{\phi}\psi\right). \tag{3}$$

From eqn. 2 it can be concluded that the rate of re-orientation thereby increases with the fibre aspect ratio AR, and the flow acceleration $\partial u*/\partial x*$. Practically, the fibre (re-)orientation is also impacted by fluctuations in the local suspension flow rate, and fibre-fibre interactions.

Peng [40] and Singh [41] performed Particle Image Velocimetry PIV experiments to measure the velocity upstream of a screen with an open area of ca. 25%. They concluded that the flow field disturbances upstream of the screen depend on the hole spacing, i.e. wire thickness S_{Open}. Velocity fluctuations larger than 10% were confined to heights of 1.5 S_{Open}, and 3 S_{Open} for S_{Open} of 530 µm, and 360 µm, respectively. Bellani et al. [42] performed PIV measurement of filtered fibre suspension matching the refraction index of the fibres and the fluid. The wire screen in their set-up had an open area of ca. 44%. The filtration velocity was varied almost a factor of 5. For all velocities, significant velocity fluctuations were confined to a region of 2 S_{Open} above the screen. This corresponded to ca. 8 times the fibre diameter D_{Fibre} upstream the screen. During the early stage in the formation of the fibre mat, this height increased to 35 D_{Fibre} (ca. 9 S_{Open}). That is a direct result from the uneven mass distribution during filtration of dilute fibre suspension. With increasing fibre mat thickness, the boundary layer thickness was found to decrease to ca. 10 D_{Fibre} (ca. 2.5 S_{Open}). Based on the recorded flow field they compared the fibre rotation time, i.e. Jeffery orbit time, to the fibre residence time within the fluctuating/accelerating flow field above the screen. They concluded that the residence time is small, and no significant re-orientation is to be expected for the open area studied. Note that a reduced open area will increase the acceleration of the flow, leading to a potentially larger change of the orientation of fibres approaching the screen.

Growth of a Fibre Mat from Fibre Stapling

Fibre stapling is another mode of fibre deposition known in paper manufacturing. A fibre is immobilized by fibre-solid friction forces on flow obstructions, e.g. pins or edges, that are small compared to the fibre. On the contrary to fibre retention, where fibre immobilization is a consequence from its retention on a screen and at least two contact points, fibre stapling starts from one contact point. Successful retention is a consequence of the force balance, i.e. inertial force, hydrodynamic force, and fibre-wall and/or fibre-fibre friction forces. Two cases are presented in Figure 3: horizontal stapling, and vertical stapling.
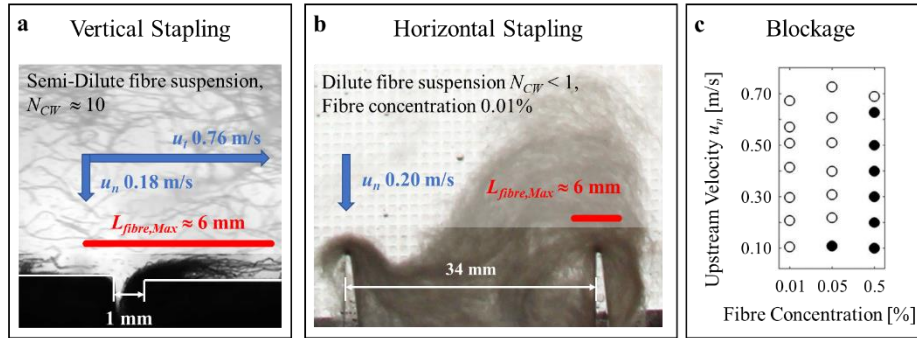
Figure 3: Fibre stapling on flow obstruction (edges). The length of the longest fibres is drawn to scale in red. The size of the opening is indicated by the white double-arrow. The suspension flow velocity in the normal u_n and tangential u_t direction with respect to the plane with the opening is indicated by blue arrows. a: Vertical fibre stapling on the downstream edge of a separation/suction channel. Image adapted with permission from Redlinger-Pohn [43]. b: Horizontal fibre stapling on pin shaped flow obstruction. c: Blockage of the opening between the pins (see b) depends on the fibre concentration and upstream velocity. Blocked cases are denoted by black dots. Image b and c are adapted with permission from Eßl [44].

Figure 3a, shows the fibre stapling observed on the edges of a separation channel used to remove near-wall fluid in a channel flow [43]. The fluid velocity is indicated by the blue arrows. Such separation channels are also found as an academic proxy for pressure screens, i.e. a typical filtration device for fibre screening [45–47]. The fibre suspension is filtered through a perforated screen basket, which is comparable to BWR strainer, with a filtration velocity u_n. The screen surface is kept clean by stirring, which results in a tangential motion u_t sweeping the screen. Olson and Kumar [45,46] describe two modes of fibre stapling on the screen that can lead to screen clogging or the blinding of single holes on the screen with respect to the fibre motion: (i) vertical stapling for high tangential velocity u_t, and (ii) horizontal stapling for high normal velocity u_n.

Vertical stapling (Figure 3a) describes fibres sweeping over the screen, for example here, where u_t is ca. $4.4u_n$. The fibres then interact with the downstream edge of the opening. Immobilization of the first fibre on the downstream edge may result from fibre-wall friction, which can be increased further by the fibre bending over the edge (a non-flexible fibre may instead rotate over the edge). The temporarily immobilized fibre may be detached from the edge and be re-entrained due to hydrodynamic drag forces acting on the fibre. Also, fibre-fibre interaction can lead to a detachment of the immobilized fibre from the edge. However, fibre-fibre interaction may also result in retention of a second fibre initiating mat growth on the edge (displayed in Figure 3a) which eventually clogs the opening.

Horizontal stapling is described by Olson [46] as individual fibres spreading over the opening supported by both edges of the opening. It thus resembles the fibre retention on a screen. Differently, Eßl [44] showed, that fibres approaching an edge, i.e. pin-shaped flow obstruction, can be retained while bending over the edge. The pin then becomes a nucleation site for a growing fibre mat. Perhaps surprisingly, the fibre mat can with time span over an

opening larger than the longest fibres in the suspension. Figure 3b presents a case of horizontal stapling that leads to coverage on an opening which is ca. 5.6 times the length of the longest fibres (a ratio of fibre length to the opening size, L_{Fibre}/D_{Open} of ca. 0.18). The ratio of the fibre length to the hole spacing, i.e. the size of the pin, L_{Fibre}/S_{Open} is far larger than 1. The blockage of the opening was studied for combinations of approach velocity u_n, and upstream fibre concentration. Cases that resulted in the blockage of the opening are denoted by a filled dot in Figure 3c. The likelihood of fibre blockage correlates directly with the fibre concentration, and indirectly with the flow velocity, i.e. increased hydrodynamic drag on the fibre counteracts stapling, but increased chance of fibre-fibre interactions benefits stapling.

Important parameters in fibre stapling are fibre-fibre, and fibre-wall friction parameters, fibre flexibility. Also, the types of collision, for example, the position of impacts and the fibre concentration, which positively correlates with the collision frequency are of importance. At higher concentrations, the fibres can also be prone to form network and this can increase the stapling probability. These parameters are difficult to quantify and even vary on an individual fibre level why a bottom-up based prediction of stapling is very challenging.

Recommendation and Suggestions from Literature

Literature suggests that already a small number of fibres from latent sources can lead to fibre mat forming on screens. The fibre mat can then filter suspended particles resulting in a high pressure loss and reduction of the flow passing through the screen. Current research efforts on Nuclear Power Plant strainers and screens focused on the description of the dependence of the pressure drop on the quantity and mixture of suspended particles. Fibrous debris is modelled from generated debris from NUKON® glass fibre mat insulation and are fractured glass fibres with uncontrolled length distribution. The glass fibre debris classification follows appearance and sedimentation velocity. It is noted that larger debris is fully retained by screens, not so however class 1 debris (individual fibres), see Table 1. The description of fibre mat forming, which then leads to particle filtration that causes a large pressure loss, is neglected.

From the review of literature from pulp and paper manufacturing it is noted that two modes of mat forming exist:

(1) The retention of fibres on a screen with opening sizes smaller than the fibre length ($L_{Fibre} > D_{Open}$), and
(2) the immobilization of a fibre on flow obstructions.

Following those recommendations, a controlled (with respect to the fibre length) full factorial experiment based on the parameters L_{Fibre}/D_{Open}, and L_{Fibre}/S_{Open} was designed. The work hence extends the pioneering work of Estridge [32], and Abrams [33] on idealized mesh screens towards regions of smaller L_{Fibre}/D_{Open}. Especially for cases were stapling dominates fibre retention, hydrodynamic drag forces can impact the degree of fibre deposition and clogging of openings. Experiments are thus conducted at two flow rates. Also, the chance of fibre interaction, resulting from the given fibre concentration is of importance. Literature comparison resulted in Crowding numbers (see eqn 1) in the range $0.1 < N_{CW} < 10$ for cases involving glass fibre debris. The fibre concentration and hence N_{CW} can be lower for latent fibres only. Hence, relevant cases are most likely within the regime of individual suspended fibres.

3. Materials and Methods

Filtration Column

A vertical flow channel, or filtration column, was built for the present study. It has a rectangular cross section of 100 mm by 100 mm. The filtration column is designed to allow for a fast change of test screens, which are inserted by a cartridge. The filtration zone is 1100 mm downstream of the inlet, which is designed as a cone to establish a uniform flow profile and fibre distribution towards the screen. The section upstream of the screen is made of glass to provide optical access. The screen cartridge was designed so that there is optical access all the way down to the plane of the screen (this is achieved by lifting the screen into the observation zone).

Filtration Rate and Upstream Velocity

The volumetric flow rate was set to 4 L/min and 20 L/min for the low and high velocity cases, respectively. The corresponding velocities are 6.67 mm/s and 33.33 mm/s. The upstream velocities are chosen to be similar to typical values reported in literature (reviewed Appendix A). The precise values are chosen based on preliminary experiments to capture the key fibre retention behaviour for all screens: (i) resolve in time the retention for efficient screens (a fast process that puts a limit to the maximum velocity), and (ii) capture retention for inefficient screens (a slow process that puts a limit to the lowest velocity). The ratio of 5 between the high and low flow rate corresponds directly to an increase of the strainer area by the same factor for a constant flow rate. Thus, this allows us to comment on the effect of the strainer/screen area modifications as a resolution to reduce the pressure loss [10]. The corresponding bulk Reynolds number upstream the screen based on mean velocity, channel width and the dynamical viscosity of water calculates to 667 and 3333, respectively.

Model Fibre and Fibre Suspension

The selection of a well-defined physical fibre model follows approaches in pulp and paper research [42,48]. The advantage is the control and knowledge on the fibre length of the fibre cuts. The choice of fibres follows the discussion of available literature data ([15], see Appendix A) and was guided by camera detectability. Polyamide fibres with three different lengths (Flock Depot, Hamburg, Germany), listed in Table 3, were used. The bulk of the experiments was performed with a monodisperse suspension of 2.4 mm red polyamide fibres. Longer 8 mm black polyamide fibres were added in a set of studies aiming at investigating the effect of a small fraction of long fibres together with shorter fibres. The shortest 1.2 mm red polyamide fibres were used in forming studies on fuel assemblies. Fibre properties (Table 3) are calculated based on the nominal coarseness, i.e. line density, stated by the producer and a material density of 1150 kg/m^3.

Since the fibres are not neutrally buoyant in water, we compare the fibre sedimentation velocity u_s to the upstream bulk velocity u_n to comment on the effects of sedimentation. The ratio results to ca. 0.051 for the 2.4 mm fibres for the smaller fluid flow velocity. Thus, the effects of sedimentation are small, and forced filtration is the dominant process. For high ratios of u_s/u_n, sedimentation needs to be taken into consideration. The ratio u_s/u_n of the 8 mm fibres was calculated to a maximum of 0.137. The long fibres were added as seeding fibres for the fibre mat formation at small quantity in a limited number of experiments. We note here that these fibres might not follow the fluid streamline as closely as the 2.4 mm long fibres due to their higher sedimentation velocity; in all other experiments u_s/u_n < 0.052.

The bulk of the experiments were conducted at a crowding number N_{CW} (see eqn 1) of 0.5. This choice was guided by the literature reviewed above and analysed further in Appendix A. For some cases, additional experiments were performed at lower and higher crowding numbers N_{CW} of 0.1, and 5, respectively.

Table 3: Properties of model fibres. The ratio u_s/u_n compares the fibre sedimentation velocity to the fluid velocity towards the screen.

L_{Fibre} [mm]	Coarseness [tex]	D_{Fibre} [mm]	AR [-]	Upstream Velocity u_n [mm/s]	Max. Settling Vel. u_s [mm/s]	u_s/u_n
1.2	0.09	0.010	120	6.67	0.17	0.026
				33.33	0.17	0.005
2.4	0.33	0.019	126	6.67	0.34	0.051
				33.33	0.34	0.010
8	2.2	0.049	162	6.67	0.92	0.137
				33.33	0.92	0.027

Filtration screens

Plates with staggered holes and rectangular wire meshes, both found as strainer and screens in BWR and PWR, were used in the experiments (see Figure 4a). The test screens, listed in Table 4, were selected or manufactured with respect to a fibre length of 2.4 mm. The bulk of experiments were performed with staggered hole plate screens, laser cut from 1 mm thick PMMA (Nordbergs Tekniska AB, Sweden). Those were manufactured following Rv DIN 24041 (staggered hole plates) covering the four combinations for a full factorial test of the parameters, L_{Fibre}/D_{Open}, and L_{Fibre}/S_{Open} (grouped in Table 4). The ID label follows the norm stating the opening size D_{Open} and the hole pitch T (see Figure 4a). With respect to the fibre length those are:

- Regime I: $L_{Fibre}/D_{Open} > 1$, and $L_{Fibre}/S_{Open} > 1$: Small holes with small spacing.
- Regime II: $L_{Fibre}/D_{Open} < 1$, and $L_{Fibre}/S_{Open} > 1$: Large holes with small spacing
- Regime III: $L_{Fibre}/D_{Open} < 1$, and $L_{Fibre}/S_{Open} < 1$: Large holes with large spacing
- Regime IV: $L_{Fibre}/D_{Open} > 1$, and $L_{Fibre}/S_{Open} < 1$: Small holes with large spacing

An additional set of experiments was performed with two wire meshes with geometrical characteristics comparable to the hole plates. Typically, wire meshes are woven from a thin (metal) thread, so that the hole spacing S_{Open} is small compared to the hole size D_{Open}. The mesh ID number states the number of openings for one linear inch of screen. The geometrical characteristics of the plates and meshes listed in Table 4 (6 plates with circles and 2 meshes with squares) are indicated in Figure 4b together with the lines separating regimes I-IV. Except for the obvious difference in design, the surface of the wire meshes is rougher, resulting from the wire weaving, whilst the hole plates have a smooth surface. The relative

open area A_{Open}, which is the ratio of the open, i.e. hole, area to the total screen area, is stated in Table 4.
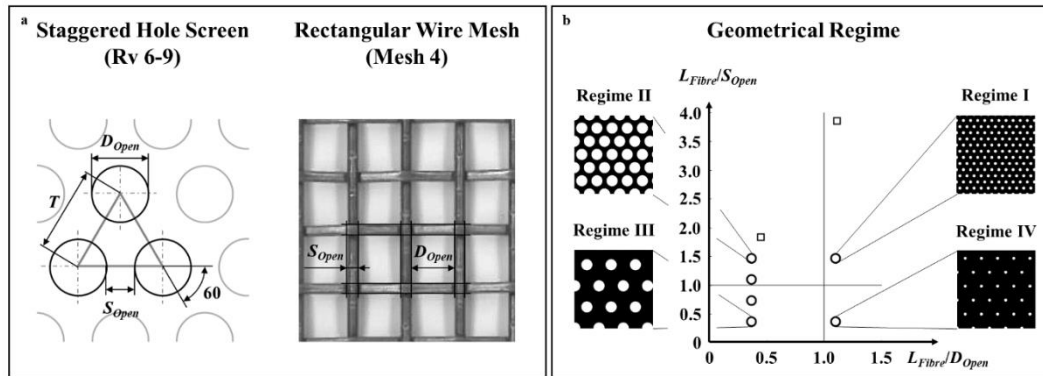

Figure 4: a: Schematic sketch of the staggered hole plate, and rectangular mesh. The mesh displays the knuckles from the weaving. b: Screens grouped into regimes based on their geometry L_{Fibre}/S_{Open}, and L_{Fibre}/S_{Open}.

Table 4: Dimension of the staggered hole plates, and wire meshes.

ID	D_{Open} [mm]	S_{Open} [mm]	T [mm]	L_{Fibre}/D_{Open}	L_{Fibre}/S_{Open}	A_{Open}	Regime
Rv 2-3.5	2.0	1.5	3.5	1.2	1.6	0.29	I
Mesh10	1.98	0.57	-	1.2	4.2	0.60	
Rv 6-7.5	6.0	1.5	7.5	0.4	1.6	0.58	II
Rv 6-8	6.0	2.0	8.0	0.4	1.2	0.51	
Mesh4	4.91	1.2	-	0.5	2.0	0.65	
Rv 6-9	6.0	3.0	9.0	0.4	0.8	0.40	III
Rv 6-12	6.0	6.0	12.0	0.4	0.4	0.23	
Rv 2-8	2.0	6.0	12.0	1.2	0.4	0.06	IV

Fuel Assembly
A model of the PLUS7 fuel assembly fitting the filtration column was made by 3D printing. The first layer of the protective grid of the PLUS7 fuel assembly is a screen with circular and elliptical openings. The size of the circular openings $D_{FA,Circle}$ is 4.95 mm, which also equals the minor axis of the ellipse. The major axis of the elliptical openings $D_{FA,major}$ is 7.44 mm. The smallest hole spacing S_{FA} is 1.48 mm. The detailed design of the fuel assembly is described in Appendix B.

Visual Tracking of Fibre Retention on Screen and Evaluation of the Screen Coverage
Fibre retention was quantified as the growth of the fibre mat as a function of specific filtration volume, i.e. the total volume V passing a screen with a given surface area A:

$$v = \frac{V}{A} = \frac{\dot{V}}{A} t = u_n t . \tag{4}$$

The specific filtration volume v was calculated from the upstream velocity u_n and the filtration time t. In eqn (4), $\dot{V}$ is the flow rate. The specific filtration volume v can be interpreted as the total height of the suspension that has passed through the screen.

The filtration process was recorded with a Nikon D7100 camera (Nikon Corporation, Japan) at a rate of 25 fps, and a resolution of 1080 pixel by 1920 pixel. Screen coverage was recorded at two camera inclinations, i.e. the angle between the optical axis of the camera and the screen plane. Recordings at the lower angle captured more details of the fibre deposition mechanism as fibres approach the screen. Recordings at the higher angle were the closest possible to a screen parallel view. Those were used to evaluate the integral screen coverage with time t, or specific volume v that passed the screen. Image post-processing is explained in Figure 5, with the case Rv 6-7.5, u_n of 6.67 mm/s as an example.
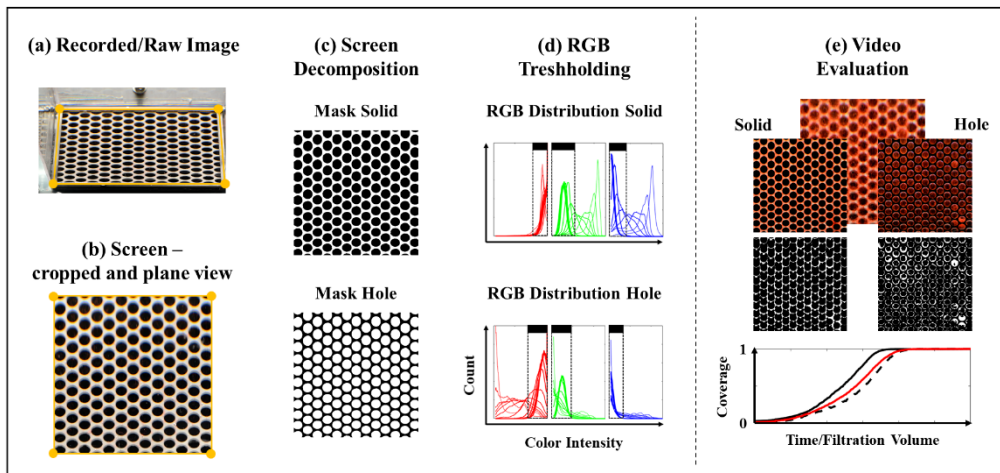
Figure 5: Image and video post-processing. Step (a) to (d) describe the post-processing strategy: raw image split into screen solid, and screen hole components. Thresholds on the RGB values are set to determine if a pixel is a fibre or not. (e) summarizes the post-processing on a single frame: fibre on screen solid (solid black line) and screen hole (dashed black line) are separated. The total screen coverage curve (solid red) is calculated from those two.

As mentioned, fibre deposition was filmed at an angle resulting in images out of the screen plane (Figure 5a). The images were first projected onto the screen plane (Figure 5b) imposing the constriction that the screen is square, i.e. the four corners of the screen in the raw image (Figure 5a) must describe a square (Figure 5b). The screen was then cropped to 90% of its size, cutting the wall area from the evaluation. Based on the first image, which captured the empty screen, masks for the *solid* screen, and *hole* screen were generated (Figure 5c). This step was initially necessitated to compensate for differences in the background illumination, where the white screen showed initially high colour intensity, and the hole showed lower colour intensity. As a bonus, the decomposition allowed us to separate the

coverage of the holes and solids. Following, the change in RGB (red, green, blue) colour intensity for the screen and hole with time was used to determine when individual pixels were covered with fibres (Figure 5d). Threshold values were set based on the max/min recorded colour intensity (between 0 to 255) and are indicated by the box with the black bar in Figure 5d. The screen coverage was evaluated accordingly as shown in Figure 5e where the binarized solid and hole coverage based on the RGB threshold values are shown at a given instant. Finally, the video was summarized by curves showing coverage as function of v or time t. Such curves are also shown in Figure 5e where solid (black solid line), hole (black dashed line) and total (red line) coverage with time, or specific filtration volume v. The coverage of the full screen was calculated as the area-weighted sum of the solid and hole coverages.

The experimental procedure for each case was: (i) filling the column with water and starting the flow at a given flow rate, (ii) adding the fibres, (iii) starting the image recording. The lag time between the start of the image recording and the approach of the first fibres on the screen varied with a few seconds between the experiments. The onset of the detected accumulation of the first fibres on the screen may thus differ slightly. Hence, we determine the screen coverage rate as the slope of coverage curve between 0.3 and 0.7, and the total filtration time (expressed as a specific filtration volume to compare between flow velocities) between coverage of 0.05 and 0.95.

4. Results

Before we turn to the details of the screen coverage, we first present a series of snapshots in Figure 6 for selected experiments in regime II (Rv 6-7.5), and regime IV (Rv 2-8). These are cases with holes larger than the fibres length and small solid area (regime II) and holes smaller than the fibre length and large solid area (regime IV).

The basic questions are two: (i) will the screen be covered with fibres at all, and if so (ii) how long does it take? The time and the specific filtration volume v stated in the images in Figure 6.
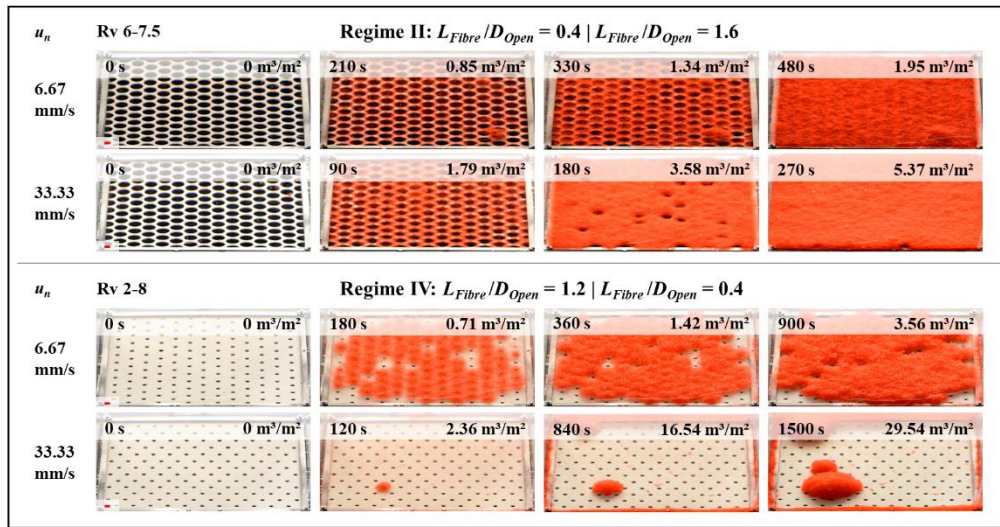
Figure 6: Snapshot time series from video recordings for two screens and approach velocities by fibres (red colour). The fibre length is indicated by the red bar in the first snapshot per series, i.e. 0 s, left-lower corner. The filtration time and corresponding filtered specific volume v per snapshot are stated. Upper two rows: Rv 6-7.5 (Regime II, large holes). Solid screen area covers with fibres followed by the blockage of the holes thereafter. Lower two rows: Rv 2-8 (Regime IV, large spacing). Screen holes get plugged by fibres followed by screen coverage thereafter. High approach velocity hinders holes plugging.

Surprisingly, it was the screen with holes larger than the fibre length that was covered easily by a fibre mat and not the screen whose holes are smaller than the fibre length. The screen with large holes is eventually covered for both the low and high velocity case. In the case with small holes, the approach velocity makes the difference screen coverage and no screen coverage (with less coverage for the high speed). Apparently, the collection of fibres on screens of various design is not straight forward, and an argument in fibre deposition must be given to the hole spacing: L_{Fibre}/S_{Open}.

Before we present the details for each of the 8 screens, we will compare and discuss the fibre mat formation of the screens tested in this study. A summary of the recorded screen coverage is given in Figure 7. The results are grouped into regime I-IV and large differences in observed screen coverage behaviour is observed. The thin lines with open symbols represent low approach velocity u_n of ca. 6.67 mm/s, and thick lines with filled symbols represent high approach velocity u_n of ca. 33.33 mm/s. Solid lines and dashed lines represent the laser cut screen. Dash-dotted lines represent the cases of Mesh4 and Mesh10. The line colour benefits the identification of the four regimes.

Screens with $L_{Fibre}/S_{Open} > 1$ were all covered by a fibre mat (red and blue curves). The process was quick for regime I, $L_{Fibre}/D_{Open} > 1$, with nearly no difference between Mesh10, and Rv 2-3 to each other and with respect to the approach velocity even though the screens differed noticeably in L_{Fibre}/S_{Open} being 4.2, and 1.6, respectively apart from the hole geometry. Coverage was achieved by v smaller than 1 m³/m² of the given suspension.

The coverage for screens of regime II, $L_{Fibre}/D_{Open} < 1$, was sensitive on L_{Fibre}/S_{Open}, and to the flow rate. The specific filtration volume at which full coverage was reached decreased with decreasing L_{Fibre}/S_{Open} and increasing approach velocity u_n. Furthermore, the impact of the flow rate seemed to increase with decreasing L_{Fibre}/S_{Open}. In particular Mesh4 was quickly covered by a fibre mat. The specific filtration volume necessary for full coverage for this Mesh4 was comparable to Mesh10 and Rv 2-3 in regime I. Larger specific filtration volumes (implying that more fibres pass the screen) were needed for Rv 6-7.5 and Rv 6-8. Especially for Rv 6-8 at u_n of nominally 33.33 mm/s a large specific filtration volume was needed to obtain full coverage. In particular, it took a long time to cover the last 30% of this screen.
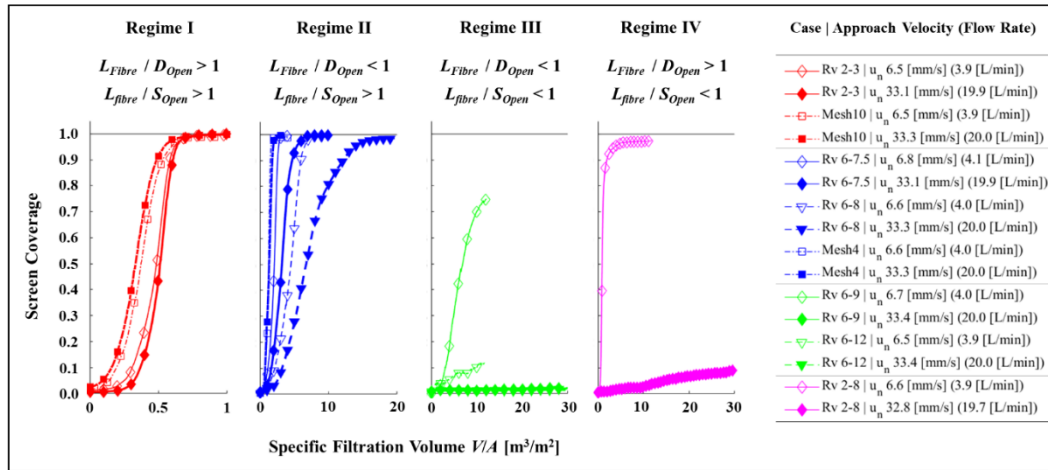

Figure 7: Screen coverage over the filtered specific volume of the tested screens (see Table 4). Results are grouped per regime (regime I: red, regime II: blue, regime III: green, regime IV: magenta). Open symbols denote the lower approach velocity, and filled symbols denote the higher flow rate of each screen setting. Hole screens are denoted by solid and dashed lines. Meshes are denoted by dash-dotted line. The exact flow rate and case setting are listed in the figure legend.

Following the decrease of L_{Fibre}/S_{Open} crossing into regime III, $L_{Fibre}/S_{Open} < 1$, we find that none of the screens were completely covered within the experimental time. There were fibres collected on Rv 6-9 at the low approach velocity of u_n ca. 6.67 m/s, but the coverage rate flattened, and full coverage was not reached. There is also some fibre collection on screen Rv 6-12 for low approach velocity with a coverage of ca. 10% at the end of the measurement. No fibres were collected for high approach velocities.

Regime IV, $L_{Fibre}/D_{Open} > 1$, and $L_{Fibre}/S_{Open} < 1$, shows high sensitivity on the flow rate, or screen approach velocity u_n. At a low flow rate, the screen was fast covered with fibres, however not fully, the curve flattens out at a high but not complete coverage. With an increased flow rate, coverage was very slow. Only 10% of the screen was covered after a specific filtration volume of 30 m³ per m² of the given suspension.

The comparison of the screen coverage for each tested screen in Figure 7, strengthened the first impression drawn from Figure 6: fibre retention differs significantly between the

screens. The geometrically based classification into regimes may in fact also describe different regimes of fibre retention on the screen. The underlying mechanisms will now be discussed in detail for each screen. The structure of Figure 8 to Figure 15 (one figure per screen) are identical, and explained in Figure 8: (a) and (b) display the integral screen coverage with values on the coverage rate and specific filtrated volume v for the lower approach velocity in (a), and the higher approach velocity in (b). Below, snapshots of a section of the screen detailing on the deposition mechanism are given in (c)-(f). The time instances of the snapshots are marked in the integral screen coverage by the circles. For cases with no coverage, only one screenshot corresponding to the end of the measurements at high v is given. Each regime is given a name characterising the retention mechanism.

Regime I: Fibre-Hole Probability Retention

Figure 8c shows the fibre deposition on Rv 2-3.5 (L_{Fibre}/D_{Open} 1.2, L_{Fibre}/S_{Open} 1.6) for u_n 6.5 mm/s at an early stage. Fibres bent over the solid spacing between two holes, as well as bridged the holes. Shortly thereafter, Figure 8d, fibres had accumulated but foremost on the holes, and to a lesser extent on the solid. This description is comparable to fibre probability retention. The suspension had to pass through the holes, and hence, fibres were directed to the holes which comprise 29% of the screen surface. The fibre on the hole resist bending due to the hydrodynamic drag and formed a fibre mat. The fibre mat grew on the hole and the solid, leading to fast screen coverage.
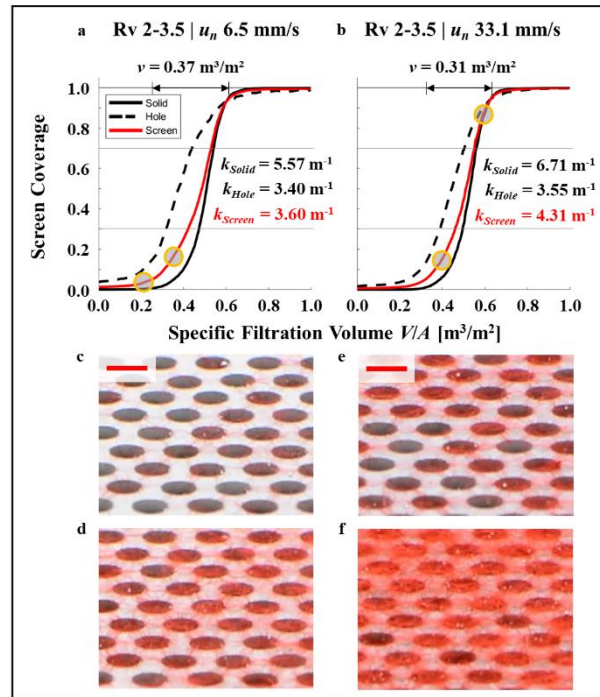

Figure 8: Screen coverage over filtered specific volume v of Rv 2-3.5 for two approach velocities u_n: low in the left row (a, c-d), and high in the right row (b, e-f). The dashed black, solid black, and solid coloured curves denote the coverage of the screen solid, the screen hole, and the whole screen (corresponding to Figure 7), respectively. The coverage rates between 0.3, and 0.7 are stated in the graphs. The specific volumes to increase coverage from 0.05 to 0.95 are stated above the graph (the range is indicated by the black double arrow in the graph). The transparent grey dots in the graph denote the instants of the snapshots below. The upper snapshot (c, and e) are earlier. The red bar in the upper snapshot corresponds to the fibre length of 2.4 mm.

The screen coverage rate k_{Screen} and specific filtration volume v were independent of the approach velocity u_n in the tested range (Figure 8a-b). In both cases, screen coverage was reached after ca. 0.3 to 0.4 m³/m². Also, the snapshots, Figure 8c-f, for both flow rates are comparable.

Figure 9c-f presents snapshots of the fibre deposition on the screen Mesh10 (L_{Fibre}/D_{Open} 1.2, L_{Fibre}/S_{Open} 4.2) for approach velocities, u_n 6.5 mm/s, and u_n 33.1 mm/s. The approach velocity had no impact on the screen coverage for Mesh10. Fibres were found to deposit on the solid and the hole relative uniformly. Coverage of the screen was fast. The coverage rate of the hole, k_{Hole}, of Mesh10 was comparable to Rv 2-3.5, as was the geometrical parameter L_{Fibre}/D_{Open}, which is 1.2 for both cases. The Mesh10 solid coverage followed the hole coverage more closely and at a comparable rate. That differed from Rv 2-3.5 where solid coverage lagged slightly in the beginning but, reached total coverage fast. We assume that these details of the hole and solid coverage is a fingerprint of the hole distribution and shape of the solid. Detailed quantification of the flow field was out of the scope of the present study. Nevertheless, some possible explanations to these differences will be discussed in the chapter "Fibre Rotation in an Accelerating Flow Field".
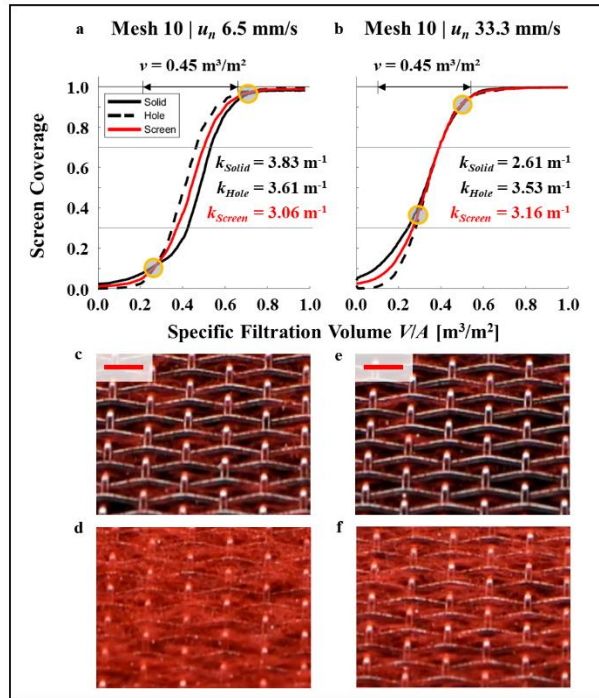

Figure 9: Screen coverage over filtered specific volume v of Mesh 10 for two approach velocities: low in the left row (a, c-d), and high in the right row (b, e-f). Labelling follows Figure 8.

We conclude that both Mesh10, and Rv 2-3.5 followed the fibre probability retention which depends on the fibre orientation and geometrical pairing of L_{Fibre}/D_{Open}. The coverage of the screen was quick and within v of 0.5 m³/m².

For screens in regime I, fibres stapled on the solid, but more significant to the screen coverage were fibres retained on the holes. Regime I may thus be labelled fibre-hole retention or fibre-hole probability retention.

Regime II: Fibre-Solid Stapling

Figure 10c shows the fibre deposition on the screen Rv 6-7.5 (L_{Fibre}/D_{Open} 0.4, L_{Fibre}/S_{Open} 1.6) for u_n 6.8 mm/s at an early stage. Fibres bent over the solid spacing between two holes, however, failed to cover the hole due to their small length (since $L_{Fibre}/D_{Open} = 0.4$ the fibres cannot span over the hole). The fibre-solid interaction in regime II was comparable to the early stage fibre-solid interaction in regime I for the staggered hole plate screen, both being within $L_{Fibre}/S_{Open} > 1$. With increasing v more fibres stapled on the solid forming a fibre mat (Figure 10d). This fibre mat aided in the retention of approaching fibres. Eventually, the screen holes got covered as a consequence of the fibre mat growing from the hole circumference inwards (for the circular hole in the staggered hole plate screen). Figure 10a shows, that the solid was covered before the holes with a larger lag of the hole coverage for the higher approach velocity. The coverage rate of Rv 6-7.5 was a factor of approximately 4-5 lower compared to Rv 2-3.5 and Mesh10. Fibre retention in regime II followed a fibre stapling process (compare Figure 3b).
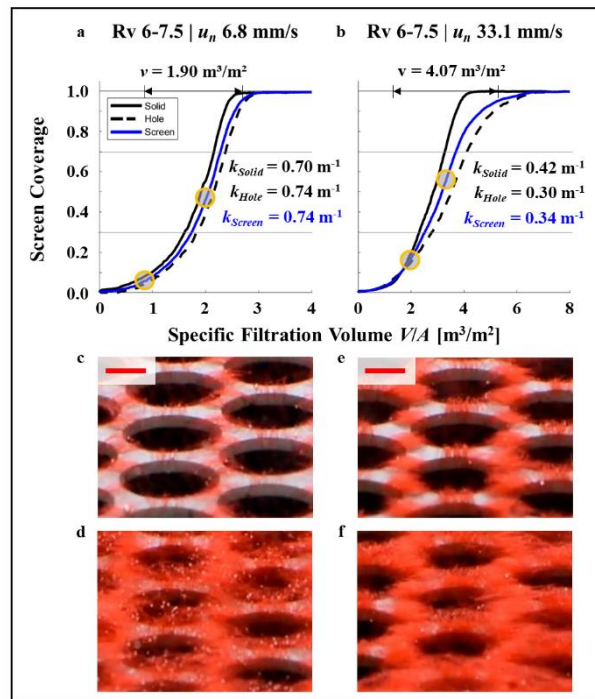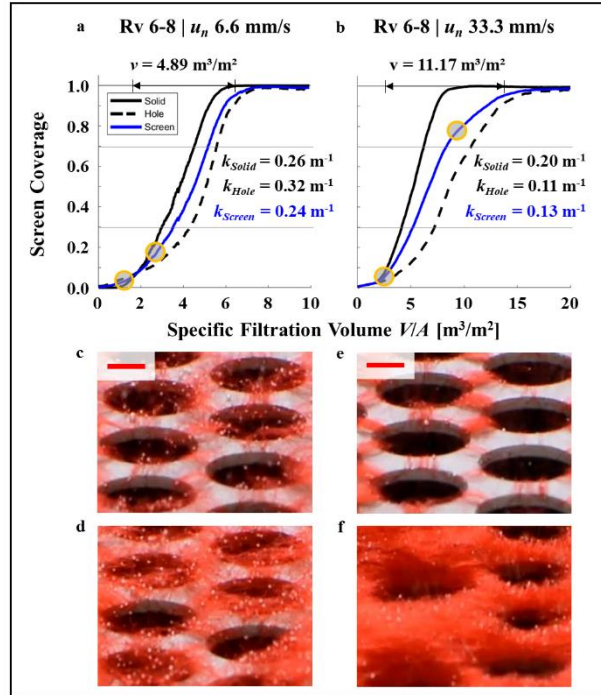

Figure 10: Screen coverage over filtered specific volume *v* of Rv 6-7.5 for two approach velocities: low in the left row (a, c-d), and high in the right row (b, e-f). Labelling follows Figure 8.

In line with the conclusion that screen coverage in regime II followed fibre stapling was the negative impact of the approach velocity u_n on the screen coverage rate. From the comparison of snapshots, Figure 10c-f, it can be taken that: (i) fibre stapled on the solid spacing, (ii) and formed a fibre mat that covered the hole with time. The rate of fibre stapling on the screen, and coverage of the hole was lower for higher u_n (compare Figure 10a to Figure 10b). The hydrodynamic drag on a fibre retained on the screen and the inertia of approaching fibres increase with u_n. In contrast, the fibre-solid, and fibre-fibre friction force can be regarded as independent on u_n. The consequence is an increased likelihood of redispersion at higher velocity. Further, the comparison of the coverage plots in Figure 10a, and b, shows a flattening of the coverage curve for higher hole coverage, i.e. 0.8 only for the u_n. The series of snapshots presented in the two top rows of Figure 6, present a stochastic hole

coverage for Rv 6-7.5. The local flow velocity during hole coverage must increase at the remaining open holes due to the decrease in open area due to the covered holes. Thus, also acceleration, fibre inertia, and hydrodynamic drag on deposited fibres increased locally for transient screen coverage. This is in line with the PIV measurements by Bellani *et al.* [42]. Hindered fibre stapling at increased velocity u_n is in accordance with observations documented in the literature, for example by Eßl [44].

Results for Rv 6-8 (Figure 11, L_{Fibre}/D_{Open} 0.4, L_{Fibre}/S_{Open} 1.2) followed Rv 6-7.5 (Figure 10) qualitatively. The coverage mechanism was stapling, and fibre deposition started from the solid (Figure 11c, e). The geometrical differences between Rv 6-8 and Rv 6-7.5 were a reduced open area A_{Open} by 12%, and a reduced fibre surplus length, i.e. $L_{Fibre} - S_{Hole}$, by 66%. Hence, a fibre retained on the solid pointed into the hole and bent over the solid edge to a lesser extent. Fibre fixation was thus less probable, resulting in a lower solid coverage rate. Also, more fibres were needed to form a mat growing into the hole from the screen. The impact of the approach velocity u_n on the screen coverage was increasing from Rv 6-8 to Rv 6-7.5, with decreasing L_{Fibre}/S_{Open} and the lag between solid and hole coverage increased. Hole coverage started after the solid was covered at higher upstream velocity u_n. This is illustrated by the snapshot displayed in Figure 11f.

Figure 11: Screen coverage over filtered specific volume *v* of Rv 6-8 for two approach velocities: low in the left row (a, c-d), and high in the right row (b, e-f). Labelling follows Figure 8.

Coverage of Mesh4 (L_{Fibre}/D_{Open} 0.5, L_{Fibre}/S_{Open} 2.0), Figure 12a-b, followed stapling mechanism showing (i) hole coverage tailing solid coverage, and (ii) a negative impact of an increased approach velocity u_n on the screen coverage rate. The fibre surplus length was 33% higher compared to Rv 6-7.5. In line with the previous observation, this increase resulted in a higher screen coverage rate. However, also the ratio of L_{Fibre}/D_{Open} was higher by 25%, and the open area ratio was higher by 12%. Both differences benefit fibre deposition on Mesh4 as compared to Rv 6-7.5. The screen shape, i.e. smooth round wires versus sharp edges of the holes, differed as well and can be expected to impact the fibre deposition. Hence, the wire mesh (Mesh4) could not be compared to the staggered hole plate (Rv 6-

7.5) based on the evaluation of a single parameter. The trends observed when comparing Rv 6-7.5 and Rv 6.8, however, were continued. Figure 12c-f display the expected coverage behaviour: fibre deposit on the mesh wire growing into the hole covering the screen with time, or v.

Figure 12: Screen coverage over filtered specific volume v of Mesh 4 for two approach velocities: low in the left row (a, c-d), and high in the right row (b, e-f). Labelling follows Figure 8.

Concluding the observations on screens in regime II, fibre stapled on the solid growing inwards and covering the holes with time. Regime II may thus be described as fibre-solid stapling, or screen fouling. The specific filtration volume needed to reach full coverage is considerable larger in regime II compared to regime I.

Regime III: Fibre-Screen Passage

The screen Rv 6-9 (L_{Fibre}/D_{Open} 0.4, L_{Fibre}/S_{Open} 0.8) gives a reduction in L_{Fibre}/S_{Open} compared to Rv 6-8 and brings us into regime III. The fibre-screen interaction of Rv 6-9 (Figure 13) was comparable to Rv 6-8 (Figure 11). Although the fibres were shorter than the solid hole spacing, some fibre were retained. For the lower approach velocity, u_n of 6.7 mm/s, the solid was covered by fibres with time (Figure 13a and Figure 13d displays this coverage of the solid). Starting from the hole edge, fibres grew in over hole. However, within the maximum observation time of 30 min, corresponding v of ca. 12 m³/m², the holes were not fully covered. Towards the end of the observed time, the hole coverage curve flattened, and it can be expected that the holes remain open for a very long, if not infinite, time if longer experiments are run. The total screen coverage presented is mainly the coverage of the 60% of the screen that is solid. The qualitative behaviour of fibre stapling on the solid discussed for regime II seems to be valid also for regime III. However, the magnitude, or the quantity of retained fibres, was too small to result in the full clogging of the holes. Hence, the screen remained open.
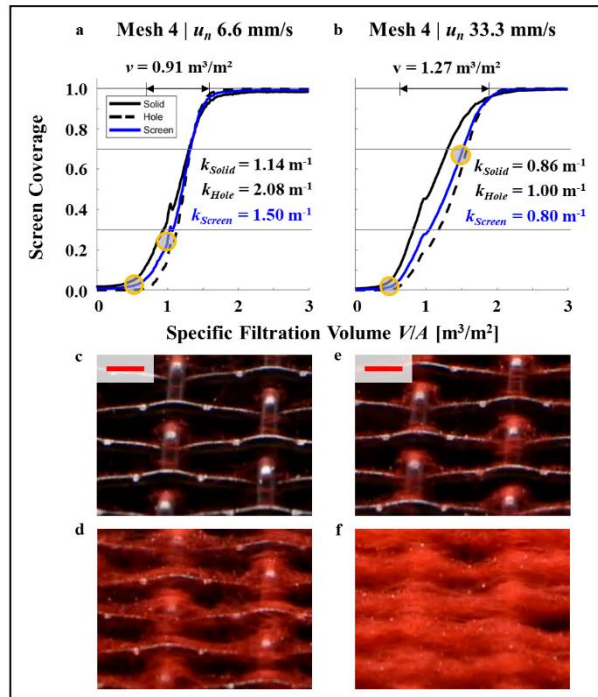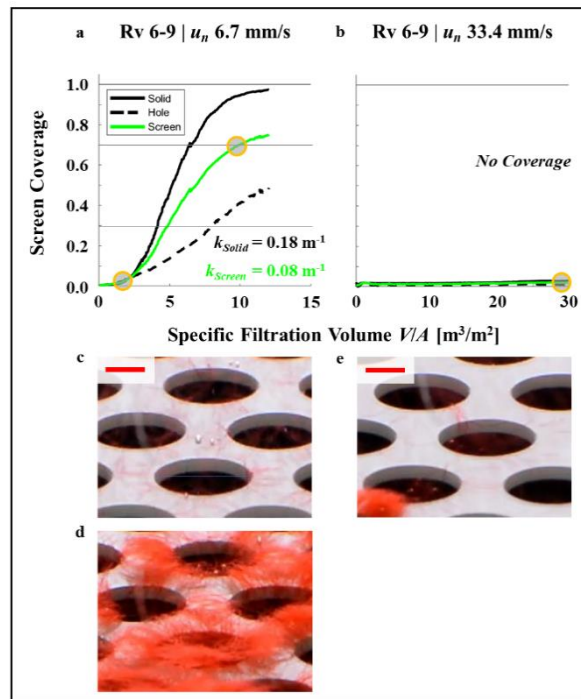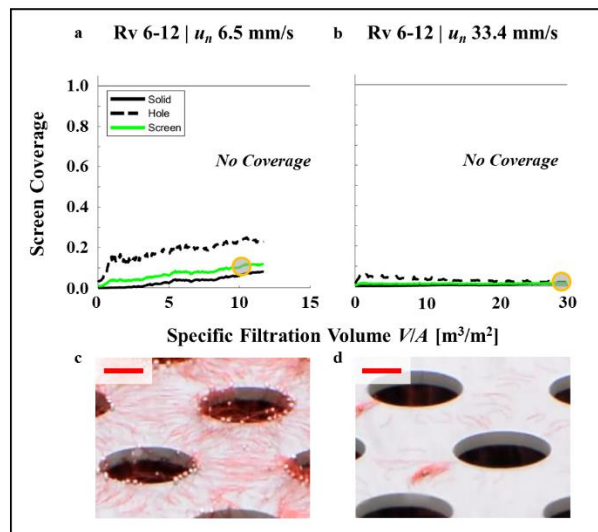

Figure 13: Screen coverage over filtered specific volume *v* of Rv 6-9 for two approach velocities: low in the left row (a, c-d), and high in the right row (b, e). Labelling follows Figure 8.

This becomes more apparent at higher approach velocity u_n of 33.4 mm/s. Fibres interacting with the solid screen remained entrained in the suspension and were prevented from deposition. A few single fibres, or small bundles of fibres, which resulted in negligible screen coverage, were collected on the solid. The screen remained basically clean within the observed time, which corresponded to v of 30 m³/m².

Further decrease of L_{Fibre}/S_{Open} to Rv 6-12 (L_{Fibre}/D_{Open} 0.4, L_{Fibre}/S_{Open} 0.4), Figure 14, resulted to a reduction of fibre deposition on the solid also at the slow approach velocity. A few fibres either (i) deposited on the screen aligned perpendicular to the edge of the hole, aligning with the expected fluid flow towards the opening, or (ii) bent over hole edge (Figure 14c-d). The deposition pattern of fibres was also observed for cases at early stages in

regime II, and regime I. In fact, the first fibres appearing on the screen aligns in the expected flow direction for all cases.

Figure 14: Screen coverage over filtered specific volume *v* of Rv 6-12 for two approach velocities: low in the left row (a, c), and high in the right row (b, d). Labelling follows Figure 8.

A small amount of fibres deposited on the solid at the lower approach velocity u_n of 6.5 mm/s. The holes remained open except for fibres that bent over the edge. For increased approach velocity u_n of 33.4 mm/s the screen, both the solid and hole remained clean from fibres.

In regime III, the holes of the screen always remained open even though the fibres deposited on the solid following a stapling like behaviour. Regime III may thus be labelled fibre-screen passage.

Regime IV: Fibre-Hole Probability Passage

Screen Rv 2-8 (L_{Fibre}/D_{Open} 1.2, L_{Fibre}/S_{Open} 0.4) is composed of small holes at large spacing. Compared to industrial applications, this is an untypical design. The snapshot time series (Figure 6, lower two rows) shows a larger dependence on the approach velocity compared to the other screens. At a lower approach velocity, u_n of 6.6 mm/s, most of the holes clogged followed by coverage of the solid. Figure 15c shows fibres spanning over the hole forming an initial mat on the hole. During the early stage of the experiment, it was noted that the fibre mats on some holes were washed through the screen. We speculate that deposited fibres are bent so that they pass through the hole. This can happen for events when fibres are accumulated on the hole in such a way that the hydrodynamic drag increased more than the additional support from the forming network. The fibres then bent and slid off the support on the hole edge. With time, most of the holes covered, but not all (Figure 15a). The fibre mat then grew from the holes outwards, and hence solid coverage lagged hole coverage. The hole coverage rate between coverage of 0.3 to 0.7 was fairly high, actually between the values found for regime I and regime II. The hole coverage curve flattened at ca. half of the observed time and remained stable at approximately 0.9.

Given the small open area of screen Rv 2-8, $A_{Open} \approx 0.06$, the local suspension velocity at the hole was highest for this screen. Hence, the hydrodynamic drag on the deposited fibres was also highest. Unplugging of covered holes, and restriction of a complete coverage resulted from the higher drag. Also, fluid acceleration towards the screen was highest for Rv 2-8 screen. Acceleration is known to re-orientate the fibre into flow direction (see for example Håkansson *et al.*[39]), facilitating passage through the hole. However, measurements of the fibre orientation upstream of the screen was beyond the scope of the present study. Theoretical aspects, however, will be discussed following in chapter: "Fibre Rotation in an Accelerating Flow Field".

Figure 15: Screen coverage over filtered specific volume *v* of Rv 2-8 for two approach velocities: low in the left row, and high in the right row. Labelling follows Figure 8.

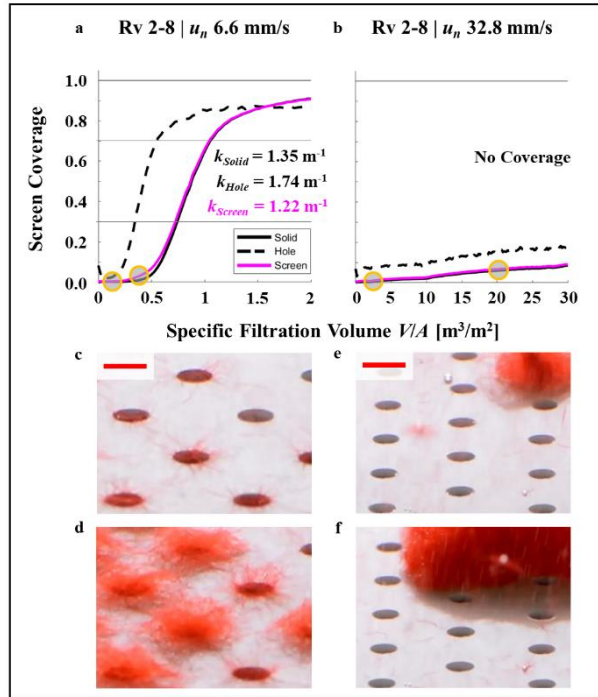No significant screen coverage was observed for the higher approach velocity, u_n of 32.8 mm/s. Recorded deposits resulted from fibres accumulating on a fibre-bundle that plugged a hole (time series in Figure 6, lowest row, and coverage curve in Figure 15b). For increased u_n, the relative velocity increase remains constant, but the hydrodynamic drag on the fibres deposited over or near the hole increased. In line with the previous argument, it appears that the hydrodynamic drag force is large enough to prevent permanent retention of fibres, which therefore are accepted (passes) through the screen.

Based on the geometrical criteria, L_{Fibre}/D_{Open}, regime IV is within the probability retention regime. Fibres deposit on the hole, which leads to the hole being covered first and the solid later. However, fibre deposits could be dragged with the flow through the screen already at the lower tested approach velocity.

The role of a non-isotropic fibre orientation distribution is not resolved for Rv 2-8. Fibre may re-orientate towards the flow direction, decreasing the probability of retention. At high velocities, the screen remained free of fibres. Regime IV may thus be labelled fibre-hole probability passage.

32

Effect of Fibre Concentration on Screen Coverage

The choice of a fibre concentration corresponding to a crowding number N_{CW}=0.5 for the base set of experiments was guided by literature. However, given the range of possible concentrations, (i) latent fibres only, and (ii) differing LOCA break sizes, this choice is still somewhat arbitrary. The fibre retention regime changes to suspension thickening for networked fibres and clogging from stapling is sensitive to the fibre concentration. A detailed investigation of the concentration regime for each screen was not performed However, in what follows we give qualitative insight into fibre mat forming at one lower and one higher fibre concentration corresponding to N_{CW} =0.1 and N_{CW} =5, respectively.
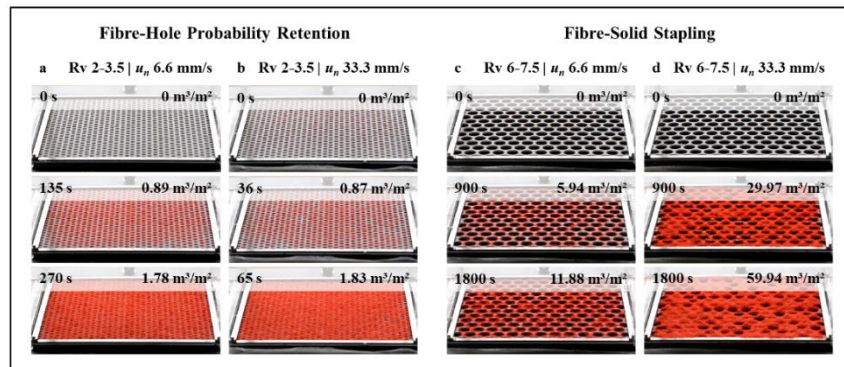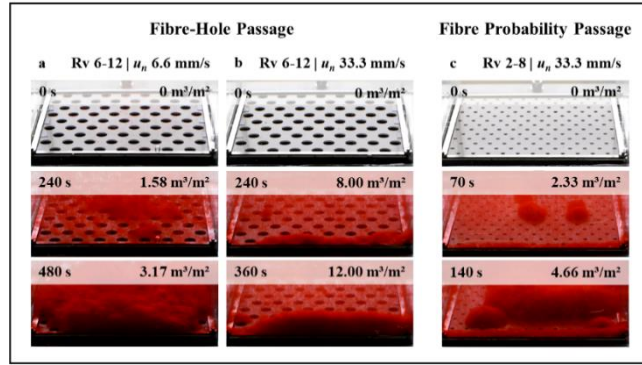

Figure 16: Fibre mat formation at a concentration corresponding to a crowding number N_{CW} of 0.1 at two approach velocities u_n stated above the cases. First two columns: fibre-hole probability retention. Last two columns: fibre-solid stapling.

Experiments at lower fibre concentration resulting in N_{CW} of 0.1, were conducted with screens that were covered with a fibre mat in the base set of experiments: Rv 2-3.5 in regime I and Rv 6-7.5 in regime II. Row a and b in Figure 16 present the coverage of Rv 2-3.5 at approach velocities u_n=6.6 mm/s and u_n=33.3 mm/s. The fibres were retained on the hole and on the solid in a manner similar to the reference case N_{CW} =0.5. The screen coverage was independent on the approach velocity u_n. Screen coverage was reached after about 1.8 m³/m², or ca. 5 to 6 times the specific filtration volume v for the 5 times higher concentrated case (Figure 8). This suggests a linear trend. This is reasonable considering a high retention probability of the first fibre and further increase of retention probability for the following fibres. The growth of the fibre mat should therefore scale with the rate of fibres approaching the screen, and thus with the fibre concentration.

Row c, and d in Figure 16 present the coverage of Rv 6-7. 5 at approach velocities u_n=6.6 mm/s and 33.3 mm/s. In both cases, the screen remained uncovered in the experimental observation time of 30 minutes. It was expected from comparison to literature (Figure 3c), that a reduction in fibre concentration would have a negative impact on the fibre mat formation. It was therefore a surprise, that the reduced concentration lead to more holes being covered at a higher velocity, an opposite observation compared to literature and findings from the base case at N_{CW}=0.5.

Figure 17: Fibre mat formation at a concentration corresponding to a crowding number N_{CW} of 5 at two approach velocities u_n stated above the cases. First two columns: fibre-hole passage. Last columns: fibre probability passage.

Experiments at a higher fibre concentration resulting in N_{CW} of 5, were conducted with screens that remained unclogged in the base set of experiments at N_{CW}=0.5: Rv 6-12 in regime III and Rv 2-8 in regime IV. Row a, and b in Figure 17 present fibre-screen inter-action of Rv 6-12 at approach velocities u_n=6.6 mm/s, and 33.3 mm/s, respectively. At the lower approach velocity, fibres in the first layer were orientated normal to the edge of the hole. With time, agglomerates, or smaller fibre bundles were retained by the screen, even-tually leading to screen coverage. At the higher approach velocity, the screen was covered from the walls of the filtration column, which should be considered a boundary defect. Within the time until the fibre mat grew from the wall, the screen remained open. The fibres in the suspension at N_{CW}=5 interact, but do not form a strong network yet (see discussion in Appendix A). At the higher velocity, the interacting fibres were dragged through the screen, but they could seed screen coverage at the lower velocity. Row c in Figure 17 pre-sent the coverage of Rv 2-8 at approach velocity u_n=33.3 mm/s. Fibre-screen interaction is comparable to the base case at N_{CW}=0.5: fibres passed through the screen, but thicker bun-dles were retained. The bundles blocked single holes and seeded screen coverage.

Impact of a small fraction of Long Fibres added to the Suspension

So far, the reported experiments were performed with a fibre length of 2.4 mm. From a practical perspective, this is an academic proxy that reveals the effect of the geometrical parameters L_{Fibre}/D_{Open}, and L_{Fibre}/S_{Open} on the formation of a fibre mat on the screen. Most real systems are expected to have a wider distribution of fibre length, especially when fibres are the result from comminution, like in cellulose pulp treatment or the wash-down of fibrous insulation material during an early stage in LOCA. It can be expected that the longest fibres in a suspension will determine the mat formation regime. In a test, we added a fraction of 8 mm fibres (two cases with 1% and 20% of the total fibres being longer) to the case Rv 6-12, originally in regime III: fibre-screen passage for the 2.4 mm long fibres (see Figure 14). The combination of 8 mm fibres and Rv 6-12, which opening and spacing was 6 mm, suggests regime I: fibre-hole probability retention. Figure 18 summarizes the results based on snapshots tracking the development of the fibre mat and a close-up detailing on the mechanism. The approach velocity of each case is denoted above the snapshots. Columns a and b are cases with an addition of 1% 8 mm fibres and columns c and d are cases with an addition of 20% 8 mm fibres. An experiment with the same amount of 8 mm fibres only, corresponding to N_{CW} =0.16, is shown in column e. The mass of each fibre length for each case is given above each column.

The close-up in Figure 18 column a shows 8 mm fibres, in black, bridging the opening. 2.4 mm fibres, in red, stapled on the 8 mm fibres that bridged the hole. The 8 mm fibres reduced the effective hole size and, given to their slender geometry, allowed smaller fibres to staple on them. Thus, a small addition of longer 8 mm fibres seeded hole coverage and led to screen coverage in a case where no coverage was obtained without the longer fibres. An increase in the concentration of 8 mm fibres led to a faster and more homogenous coverage of the screen (Figure 18 column c). The deposition rate of 8 mm fibres increased directly with its concentration (regime I). Hence, the effective opening size decreased faster what benefited the deposition of the smaller 2.4 mm fibres.

Figure 18 column b shows a case of 1% 8 mm fibre addition at high approach velocity u_n= 33.3 mm/s. The long fibres were retained on both the solid and the holes. Further on, the fibres were dragged through the holes by the suspension and washed away from the solid part of the screen. The screen is still blank after 30 minutes.

Addition of 20% 8 mm fibres led to the formation of a stronger base network on which the 2.4 mm fibres were retained. The last time instance of the case, Figure 18 column d, displays an unevenly covered screen (note that the total time in this column is a tenth of column c). This differs both from the cases of slower approach velocity (column c) and the same approach velocity but without the presence of smaller 2.4 mm fibres (column e). In both the other cases, the 8 mm fibres were homogenously distributed over the holes and covered the screen. Allowing some speculations, the reason behind this observation might be that the coverage depended on local and temporal fluctuations of the number of longer 8 mm fibres and smaller 2.4 mm that became significant during the fast coverage process with 20% 8 mm fibres. A larger local number of 8 mm fibres on the hole stabilized the net(work) formed on the hole. A larger local number of smaller 2.4 mm fibres stapling on (a smaller number of retained 8 mm fibres) increased the drag force on the total net(work) covering the hole. Depending on the flexibility and fibre-fibre friction, as well as fibre-solid friction, the net(work) could eventually bend through the screen holes and pass through the hole in the latter case.
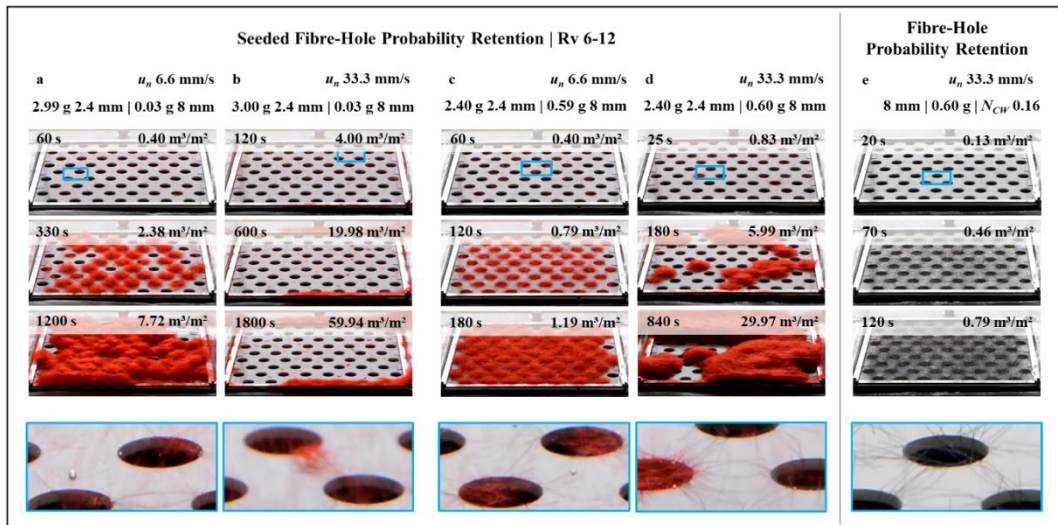
Figure 18: Fibre deposition and screen coverage for a binary mixture of 2.4 mm fibres, and 8 mm fibres on the Rv 6-12 screen. The addition of 8 mm fibres is 1% in column a and b, and 20% in column c and d. Column e shows a case with a comparable Crowding number of 8 mm fibres as in case column c and d alone. The parameters for each case are stated above the columns. The bottom snapshot in each column is a close-up on the fibre deposition from the region marked with a blue square in the top snapshot.

Fibre Rotation in an Accelerating Flow Field

From the observation of fibre deposition and screen clogging we noted differences with the approach velocity u_n and flow constriction, i.e. A_{Open}. Previously we discussed the hydrodynamic drag, which increased with u_n. Here we will discuss the impact of the accelerating flow through the screen opening on the fibre orientation, and hence the deposition probability. For that, we compare the hole coverage rate k_{Hole} for screens with $L_{Fibre}/D_{Open} > 1$ (Mesh10, Rv 2-3.5, and Rv 2-8) and compare the re-orientation time to the residence time of the fibre in the accelerating flow field. We simplify the problem to a bi-axial geometry problem, discussion the theoretical case of a fibre approaching a screen opening along the axis through the centre of the opening, i.e. the x-axis with respect to the nomenclature introduced in Figure 2. The case is sketched in Figure 19b: a fibre initially normal in the flow direction, i.e. $\phi = 90°$, would be retained on the screen. In the extensional flow field, the fibre turns into the flow and passes through the opening (from right to left in figure 19b).

Equation (3), is solved numerically for fibres with the aspect ratio AR of 2, 10, and 126. The last resembles the model fibre used in this study (Table 3). The fibre orientation distribution Ψ is initially homogenous, i.e. $\int \psi d\phi = 1/(2\pi)$, and tracked for increasing flow acceleration. The flow acceleration, i.e. $\partial u^*/\partial x^*$ is inversely proportional to the screen opening A_{Open}. Figure 19a summarizes the resulting fibre orientation distribution per screen. Distribution of AR 10 fibre and AR 126 fibre nearly fall on each other reflecting the steep increase towards 1 of the term $(1 - AR^{-2}/1 + AR^{-2})$ in equation (2) already at small AR. The fibre rotation for different AR varies less than 1% for $AR \geq 8$.
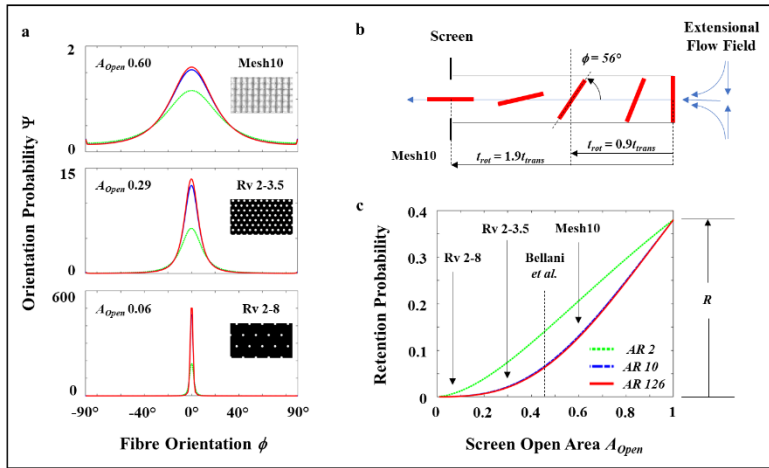

Figure 19: Fibre orientation in an accelerating flow field and the theoretical fibre retention R. a: Orientation distribution Ψ dependent on the fibre orientation ϕ for screens Mesh10, Rv 2-3.5, and Rv 2.8. Fibre aspect ratio AR is 2 (green dotted), 10 (blue dash-dotted), and 126 (red solid). b: Sketch of the fibre orientation evolution in an accelerating, extensional flow field accompanying c. The time stated below corresponds to the theoretical re-orientation t_{rot} for Mesh10 and AR 126 fibre computed from equation (2) relative to the fibre residence time t_{trans}. c: retention probability R of $L_{Fibre}/D_{Open} = 1.2$ calculated based on the fibre orientation distributions in a.

Figure 19c presents the theoretical retention probability R of a fibre with $L_{Fibre}/D_{Open} = 1.2$ based on the fibre orientation distribution Ψ after the acceleration towards the hole. The

theoretical fibre retention R in the non-accelerating flow field, i.e. $A_{Open} = 1$, results from a geometrical consideration.

$$R = 1 - \int_{-\phi_{\min}}^{\phi_{\min}} \psi d\phi \text{, with} \tag{5}$$

$$\phi_{\min} = \sin^{-1}\left(\frac{D_{Open}}{L_{Fibre}}\right). \tag{6}$$

A fibre on a screen with L_{Fibre}/D_{Open} of 1.2, is retained for inclinations ϕ from the flow direction of 56° to 90°, which gives ca. 38% for isotropically orientated fibres. This value is comparable to the values reported by Estridge for an isotropic fibre orientation distribution and thin wire grid [32], Figure 2b. It is worth to note that the sensitivity on L_{Fibre}/D_{Open} in the range between 1 to ca. 2, which equals to ϕ_{min} of ca. 30, is high. Due to the acceleration, the retention probability R decreases with decreasing A_{Open}. The curve flattens for AR 10 and for AR 126 it approaches $R = 0$ at $A_{Open} \approx 0.1$. This contradicts the fact that we observed fibre retention on the screen Rv 2-8 with $A_{Open} = 0.06$ at low approach velocities. The reason might be that there is hydrodynamic interaction between fibres and shear that reduces the aligning effect of the acceleration.

We will now compare Mesh10 to the work of Bellani *et al.*[42]. They resolved the flow field with Particle Image Velocimetry PIV for a regular mesh with D_{Open}=2 mm, and S_{Open}=1 mm. This gives A_{Open}=0.44, and D_{Open}/S_{Open}=2. The flow field was reported to be affected by the mesh at a distance of $2S_{Open}$ upstream of the mesh. They concluded that the residence time of their fibres with L_{Fibre}/D_{Open}=4.7 and 9.4, is small compared to the orbital rotation time resulting from Jeffery's equation. For our Mesh10, A_{Open}=0.6 and D_{Open}/S_{Open}=3.47. For that, it is fair to assume an even smaller disturbance than the one observed by Bellani *et al.* [42], and a comparison to their value is thus conservative. We computed from equation (2) the time to rotate t_{rot}^* from ϕ= 89° to ϕ =56° inclination of AR 126 and Mesh10 to be 1.7. That is in the range of the undisturbed residence of the fibre t_{trans} in the accelerating flow field. Such a rotation is sketched in Figure 19b. Hence, rotation may affect the early stage of fibre deposition. We found the hole coverage rate k_{Hole} increasing during the initial stage of the fibre deposition. All over, it is reasonable to assume no larger impact of fibre orientation on the coverage of Mesh10. The argument is extended to the staggered hole plate screen Rv 2-3.5. The theoretical ratio of t_{rot}/t_{trans}<1, and thus the fibre orientation in the accelerating flow field needs to be taken into account. However, the hole shape and hole pattern on the screen differ from Bellani *et al.* [42], and Mesh10. We thus tend to compare the slope of the hole coverage rate k_{Hole}, which is comparable between Rv 2-3.5 and Mesh10. Overall, the impact of fibre rotation in these cases is probably negligible.

The hole coverage rate k_{Hole} for Rv 2-8 was reduced by a factor of 5 when compared to Rv 2-3.5 and Mech10. In part, the smaller k may result from the observed unplugging of the holes during the early stage. However, also the shape of the early fibre bundles covering the holes, before the screen was covered, differed from Rv 2-3.5 exhibiting fibres in the flow normal direction.

We conclude that an orientation effect may impact the fibre retention for very low A_{Open} such as A_{Open}=0.06 for Rv 2-8 but is negligible at higher values, as demonstrated for A_{Open}=0.23 for Rv 2-3.5.

5. Screen Performances

From the experiments reported here, we can deduce a practical comment on the increase of screen surface area as a resolution to past NPP incidents [10]. For a constant volume flow rate $\dot{V}$, the ratio of the low and high screen approach velocity, $u_{n,low}/u_{n,high}$, is the inverse of the increase in screen surface area. The ratio of the total volume passing the screen until coverage is then the product of the ratio of the specific filtration time, $v_{u_n,low}/v_{u_n,high}$, and the ratio of the surface area.

The results for the fibre mat forming screens in regime I and regime II are summarized in Table 5. The comparison shows that with the increase in screen surface area, which benefited the pressure drop over the particle laden fibre mat, a larger amount of fibre suspension passes the screen before coverage. For screens in regime I, whose coverage was unaffected by the approach velocity, the increase in volume passing the screen is directly proportional to the increase in screen surface area. For screens in regime II, whose coverage rate increased with decreasing approach velocity, the ratio of the volume passing before full coverage was lower than the ratio of screen surface area, or ca. 2.5 for the tested screens.

Table 5: Effect of screen surface area ratio on total accepted volume through the screen until coverage.

	Regime I		Regime II		
	Mesh10	Rv 2-3.5	Mesh4	Rv 6-7.5	Rv 6-8
$\dfrac{u_{n,low}}{u_{n,high}}$	0.20	0.20	0.20	0.21	0.20
$\dfrac{v_{u_n,low}}{v_{u_n,high}}$	1.00	1.19	0.72	0.47	0.44
$\dfrac{A_{screen,u_n,low}}{A_{screen,u_n,high}}$	5.12	5.09	5.05	4.87	5.05
$\dfrac{V_{screen,u_n,low}}{V_{screen,u_n,high}}$	5.12	6.08	3.62	2.27	2.21

This means that more fibres will pass the strainers and continue towards the fuel assembly when the strainer surface is increased. A first resolution to decrease the amount of fibres passing the screens in the early stage may be stacking of screens, i.e. to put one screen upon another. With a modification on the screen cartridge below the observation zone, we could probe the effect of stacked screens. The spacing between the two screens was limited to 5.5 mm. That is ca. 2 times the fibre length, and ca. 4 to 5 times the hole spacing S_{Open}. No statement can be given on possible interference of the flow field between the upper, and lower screen at this point. The focus was to study additional retention thanks to the added

screen. Three different combinations of screens from regime I and regime II were tested for a high approach velocity of ca. 33.3 mm/s, and a fibre concentration corresponding to N_{CW} of 0.5.

Figure 20 shows the deposited fibre mat on the bottom screen after one filtration run. The corresponding screen coverage rate is stated above the images. For combinations where the bottom screen was more efficient, a fibre mat formed on the bottom (downstream) screen, i.e. Mesh4 on top of Rv 2-3.5, and Rv 6-7.5 on top of Mesh4. For the inverse case with the more efficient mesh on top, i.e. Mesh4 on top of Rv 6-7.5 no fibres were accumulated on the second screen. Fibre mats formed between the screens persisted backflushing, which can clean the first screen, since the fibre mat between the screens was retained by the upper screen. Upon further filtration, additional fibres were accumulated between the screens (Figure 20d).
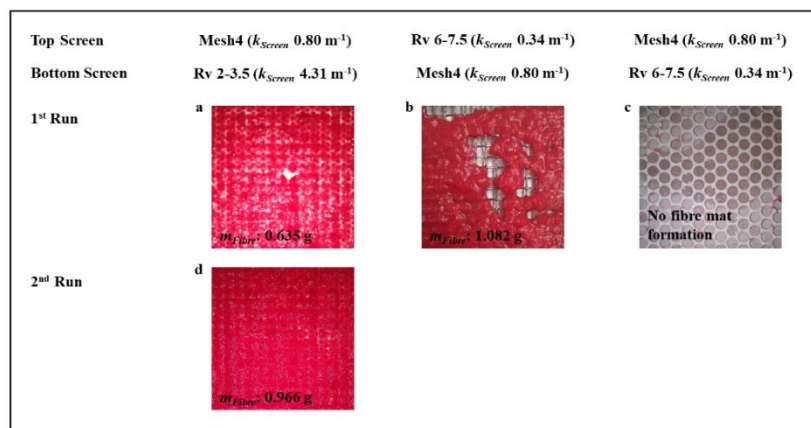

Figure 20: Fibre mat formed on a second screen twice the fibre length downstream the first screen. a-c: results for three different configurations. Screen type and screen coverage rate are stated on top. d: second run after backflushing.

In summary, an increase in surface area is beneficial to the pressure loss over the screen for long term operation. That is at the cost of an increase in the amount of fibres passing the screen at the initial stages of the filtration, i.e. during forming of the fibre mat. The amount of fibres passing the screen can be reduced by adding a more efficient screen downstream the first screen. Fibres caught on the second screen may however resist backflushing and form a permanent fibre mat caught between both screens, thus giving a high pressure drop also after back-flushing.

6. Fibre Mat Formation on Fuel Assemblies

Figure 21a-d presents a series of snapshots of fibre deposition on the model of the PLUS7 fuel assembly (see Appendix B). Clearly, there is a large qualitative dependence on the fibre length. The 1.2 mm fibres could pass through the fuel assembly, whilst the 2.4 mm fibres covered the fuel assembly forming a fibre mat. The forming of the fibre mat depended on the approach velocity u_n for the 2.4 mm fibres. The rate of fibre mat forming decreased with time and a few of the openings remained open for a longer time, thus hindering coolant flow locally. That is a direct analogy to fibre stapling documented for screens with a hole size that is larger than the fibre length, but whose hole spacing is smaller than the fibre length (regime II: fibre-solid stapling).
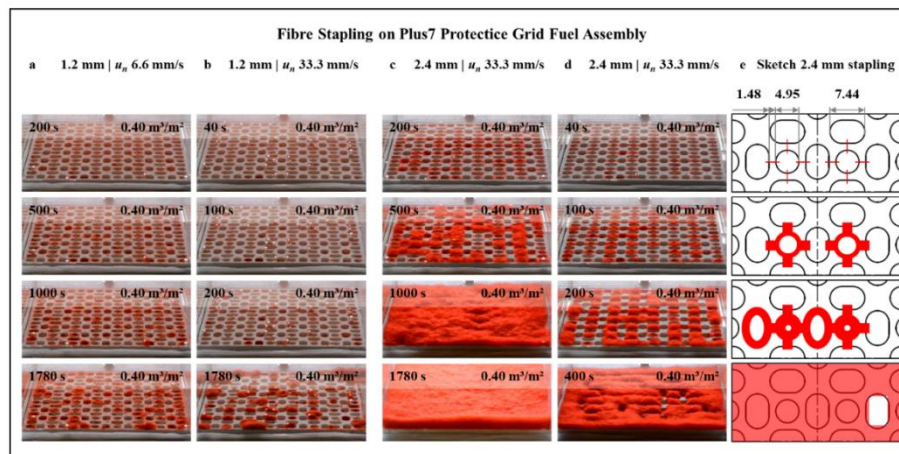
Figure 21: Fibre retention on a fuel assembly protective grid layer PLUS7. a and b: suspension of 1.2 mm fibres. c and d: 2.4 mm fibres. a and c: approach velocity u_n of ca. 6.6 mm/s. b and d: approach velocity u_n of ca. 33.3 mm/s. e: a sketch of the fibre stapling process of d.

Figure 21e sketches schematically the process of fibre mat forming from Figure 21 column d: 2.4 mm fibres, and higher approach velocity u=33.3 mm/s. The first image in Figure 21 column e states the key geometrical parameters in mm. The spacing between the openings L_{Fibre}/S_{FA}=1.62. Fibre deposited first on that spacing and the region covered by fibres grew slowly over the solid. In Figure 21 columns c and d we see the resulting pattern of the deposited fibres. From the solid, the coverage grew inwards towards the smaller openings, i.e. the circular opening. Only later in the process, the larger elliptical openings were covered with fibres. With time, the fuel assembly was fully covered by a mat of 2.4 mm fibres. For the cases shown in Figure 21 columns a and b, with a ratio L_{Fibre}/S_{FA}=0.81, the fuel assembly remained uncovered within the observation time of 1780 s (ca. 30 min).

The novelty deduced from this insight is the importance of the hole spacing. Design and selection parameters of fuel assembly are traditionally based on retention of scrap metal pieces, protection of the fuel assembly (cladding), and fluid mixing to enhance heat transfer (see for example the review on evolutionary changes in design features of advanced PWR fuel assemblies by Kim [49]). Results of this study suggest including the hole spacing as a design parameter of fuel assemblies if fibres in the coolant are to be retained or passed in a controlled manner.

With the understanding on the fibre deposition on fuel assemblies, comments can be given on literature on this matter. Suh [15], and Suh *et al.* [16] reported the formation of a fibre mat on the lower grid only for longer fibres, and on several grids for smaller fibres. The ratio of L_{Fibre}/S_{FA} was smaller for the latter case. This is related to the insights on fibre-screen stapling we showed previously, namely that a decrease in L_{Fibre}/S_{FA} results to a decrease in coverage rate. More fibres were accepted through the fuel assembly and could potentially be collected on a fuel assembly further downstream.

7. Conclusions

Fibre deposition on screens leading to fibre mat forming does not follow one retention regime but depends on the fibre length L_{Fibre} with respect to the screen opening (hole) D_{Open}, and screen hole spacing (solid) S_{Open}. Successful screen coverage from fibre deposition was achieved either by probability retention on small holes or stapling on small spacings (solid). Important factor was the combined effect of hydrodynamic forces, friction forces and fibre flexibility. The interaction of these parameters during the fibre retention process and its impact on the formed fibre mat structure were intensively researched previously for a distinct selection of screens: small opening and small spacing with respect to the fibre length [21,32,33,50] due to the importance of this case for papermaking. Fibre deposition on screens and the consequent fibre mat formation is however general and of interest for nuclear energy production. There, fibre bundles and fibres of unknown size distribution were documented to deposit on screens of differing designs. The formed fibre mat filters particle for which the pressure drop over the screen was found rising to unacceptable values [7,8,12]. Fibres passing the screen have also been found to be deposited on the fuel assembly [15,16,51]. These depositions are a risk to the safe operation of nuclear power plants in both normal operation and during LOCA.

We focused on the deposition of fibres on screens classified by their geometry in relation to the fibre length identifying 4 regimes based on L_{Fibre}/D_{Open}, and L_{Fibre}/S_{Open}. The retention of fibre bundles and fibre networks were not considered, as the retention of large, near-spherical body on a small opening is obvious. Fibre deposition on the screens was recorded and processed based on colour thresholding. The results are summarized in Figure 22 where the coverage rate (in terms of specific filtration volume) is indicated as the diameter of the circles for different screen geometries. The coverage rate for high velocities are illustrated by the top half circles and the coverage rate for the low velocity by the lower half circles. Although the regimes were distinguished purely by their geometrical relation to the fibre length, we found distinct modes of fibre deposition. Most effective was the retention of fibres in regime I, i.e. the screen coverage rate k_{Screen} indicated by the half spheres in Figure 22 is largest. Also, k_{Screen} did not differ a lot between the two tested screens in regime I.
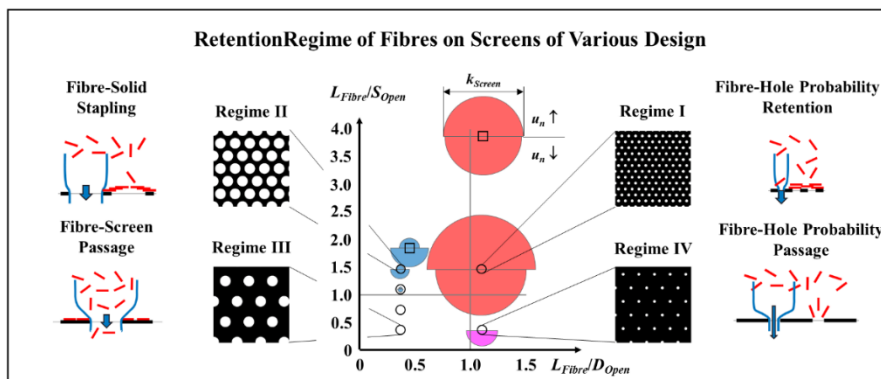
Figure 22: Retention regime of fibres on screens classified by their geometry in relation to the fibre, i.e. L_{Fibre}/D_{Open}, and L_{Fibre}/S_{Open}. Circles denote staggered hole plate screens, and squares denote wire meshes. The diameter of the upper and lower half circle is proportional to the screen coverage rate k_{Screen} [m^{-1}] for high and low approach velocity u_n, respectively. The scale for k_{Screen} is ca. 3.1 m^{-1} for Mesh10 in regime I. The labelling colour follows Figure 7. The fibre deposition mechanism per regime is sketched.

Surprisingly, also screens in regime II, which hole size D_{Open} is larger than the fibre length L_{Fibre}, was covered, but at a lower rate. The coverage rate was sensitive on the hole spacing S_{Open}. The findings per regime are summarized as:

Regime I, small holes and small spacing, retained fibres that were longer than the diameter or width of the holes. Fibres bridge the openings thanks to their length. Deposition depends on the fibre orientation with respect to the flow direction. Estridge reported that the initial retention increases with increasing L_{Fibre}/D_{Open} (Figure 2, [32]). Initial retention reaches a plateau value close to 1 for L_{Fibre}/D_{Open} of 2. Fluid acceleration upon passage through the screen opening is known to cause rotation of elongated particles, such as fibres [39] and the acceleration was reported by Bellani *et al.* to occur in a region limited to 2 S_{Open} [42] upstream of the screen. We compared fibre residence time in the accelerating flow field to the theoretical time of fibre rotation to an extent preventing retention. We concluded that orientation may have an impact on the initial screen coverage, but to be all-over negligible. The negligibility of fibre rotation in this regime could also be deduced from the comparison of two screens with different open area A_{Open} in regime I (Figure 22: square, and circle). The hole coverage rate was almost independent on A_{Open}. The concentration was found to impact the time to form a fibre mat linearly, as expected. The linear relationship was, however, deduced from two set points only. In this regime, the process to form a fibre mat is comparably fast and independent on the approach velocity, i.e. the same amount of suspension passing the screen leads to the same amount of deposited fibres. The regime was classified as fibre-hole probability retention and corresponds to the cases intensively studied in paper forming.

Regime II, large holes and small spacing, was found to collect fibres on the solid hole spacing. Subsequent fibres form a network with the first fibres eventually covering the whole screen. Fibre collection followed fibre stapling, recognised as an unwanted accumulation of fibres in cellulose pulp processing [43–46]. The negative impact of the approach velocity (Figure 22, differing coverage rate presented by the half spheres), solid hole-spacing (S_{Open}), and decreasing fibre concentration were comparable to what is reported in the literature. The fibre fixation on the solid hole-spacing resulted from fibre-solid friction upon fibre impact being larger than the hydrodynamic drag, which promotes fibre redispersion. Increased approach velocity shifted the competition between hydrodynamic drag and friction towards redispersion. Larger S_{Open}, i.e. smaller L_{Fibre}/S_{Open}, impacted the fibre-solid contact, and presumably the area over which friction acts. It is reasonable to assume that the shape of the solid impacted the fibre-solid interaction. Fibre deposition on a wire mesh (Mesh4) may thus be favoured compared to fibre deposition on staggered hole plates (Rv 6-7.5). These two screens, however, differed also in L_{Fibre}/D_{Open}, and L_{Fibre}/S_{Open} and a clear quantification cannot be deduced from the data. A smaller fibre concentration decreased the likelihood of fibre-fibre interaction and thus the rate of fibre mat growth. The regime was classified as fibre-solid stapling.

Regime III, large holes and large spacing, extends fibre stapling from regime II to cases where the flow obstruction, i.e. S_{Open}, was large compared to the fibre length L_{Fibre}. Fibre fixation on the screen was hindered, but not prevented in case of ratios close 1. The solid part of the screen was covered, but the holes remained open. Further increase in S_{Open} prevented significant stapling of fibres on the screen. An increase of the concentration in fibre-interaction regime allowed the retention as a network at low approach velocity. A weak interaction of the fibres (fibre-fibre friction at limited fibre contact points below true flocculation, or fibre networking), was enough to bridge the holes. An increase of the approach velocity hindered such retention. The regime was classified as fibre-screen passage.

Fibre mat formation in regime III was followed up by seeding the suspension with a fraction of longer fibres, which result in regime I retention on the screen. For a low approach velocity u_n, an addition of ca. 1% of the longer fibres that bridged the holes was enough to retain the smaller fibres on the screen. The longer fibres reduced the hole size, and smaller fibres stapled on the longer fibre bridging the now effectively smaller opening. An increase in long fibre content to ca. 20% (mass ratio of long fibres to short fibres of ca. 0.25) resulted in a shorter time until screen was covered. The mechanism of the initial retention of long and short fibres was comparable for higher approach velocity. However, the loading of the small fibres on top of the long fibres at the higher hydrodynamic drag caused the long fibre to bend through the hole and no coverage was achieved. Coverage was stochastic when 20% long fibres were added. With high velocity the fibre mat formation was slow compared to the low approach velocity or to the retention of long fibres only at comparable concentration. With the addition of long fibres, fibre bending through the opening is in spirit comparable to what was found for regime IV: the hydrodynamic forces are high enough to overcome the fibre stiffness.

Regime IV, small holes and large spacing, was found to be sensitive to the approach velocity. This screen geometry results in an open area A_{Open} as low as 6% for the tested case. Fibre rotation was discussed to have a negative, but not totally hindering, effect on fibre mat forming. For low approach velocity u_n a high, but not full, screen coverage was rec-orded. Fibres were bridging the openings and at early times the covered holes were found to be unplugged. We hypothesize that the high hydrodynamic drag force, which increases with the fluid velocity that is higher for screens with small open are, caused the fibres to bend and pass through the holes. The higher approach velocity prevented fibre deposition on the screen unless already created fibre bundles got stuck in a hole, allowing following fibres to be retained on this fibre bundle. The regime was classified as fibre-hole probability passage, reflecting the dependence on the fibre orientation and the fact of limited screen hole coverage. An increase in fibre concentration towards levels where fibre interactions start to occur, but below fibre entanglement and flocculation, had no impact on the cover-age rate at high approach velocity.

This report discusses fibre retention and fibre mat forming on screens classified by their geometry in relation to the fibre length. The effect of parameters like the hydrodynamic drag and fibre orientation were determined indirectly by analysing the effect of an increase in the approach velocity. The fibres were observed to bend over flow-obstructions (the solid parts of the screen) or through the screen opening (regime IV) due to increased hydrody-namic drag compared to the fibre-solid friction at increased velocity. The quantification of these is close to inaccessible in experimental studies but could be followed up by numerical studies. In numerical studies, it is easy to change parameters e.g. friction factor or fibre bending stiffness [52–56]. However, numerical studies suffer from difficulties to properly model other parameters, e.g. uneven surface roughness or fibre properties that vary. Thus, experiments that are as close as possible to the actual situation are necessary to obtain quantified and directly applicable knowledge. A key aspect in such an effort would be to sample real latent fibres and glass fibres debris on screens installed in the nuclear power plants.

Following the elevated insight in fibre deposition mechanism comments could be given on the fibre mat coverage of fuel assemblies and Emergency Core Cooling System (ECCS) strainers or screens. In order to resolve the potential issue of large pressure loss over the strainer due to coverage of fibre mats, its surface area has been increased. Hence, the area-specific fibre load and particle load decreased, leading to a reduced pressure loss. Based on the fibre mat coverage rate we could show that this will probably also lead to an increase

of the amount of fibres passing the screen before full coverage has been reached. For deposition in regime I (fibre-hole probability retention) the amount of accepted volume grew approximately linear with the increase in screen surface area. For deposition in regime II (fibre-solid stapling) the increase in accepted volume was lower than the increase in the screen surface area. Applying a second screen to boost fibre collection had mixed effects. In case of an efficient screen installed upstream a less efficient screen, only the first participated in the fibre collection. The second screen may serve other purpose but was not active in the fibre collection. In case of an efficient screen mounted downstream of a less efficient screen, fibres were also collected on the second screen effectively improving fibre retention. The fibre mat formed between both screens, however, resisted back-flushing used to clean screen upon a drop in coolant flow rate and remained between the screens.

Fibre deposition on a fuel assembly model was seen to be analogous to fibre deposition on screens. We showed that for the PLUS7 protective grid a fibre stapling process leads to partial coverage by a fibre mat, leading to an uneven distribution and even partial blocking of the coolant flow. It could be useful to include the parameters L_{Fibre}/D_{Open}, and L_{Fibre}/S_{Open} into consideration when evaluating fuel assembly designs.

8. References

1.   Deutsch, N. The Changing Role of Nuclear Power in the European Union: Reflections from Official Scenarios Released before and after the Fukushima Daiichi Accident. *Theory, Methodol. Pract.* **13**, 17–36 (2017).

2.   European Commission. *Energy Roadmap 2050*. (2012). doi:10.2833/10759

3.   International Atomic Energy Agency. Energy, Electricity and Nuclear Power Estimates for the Period up to 2050. 150 (2018).

4.   International Atomic Energy Agency. *Nuclear Power Reactors in the World*. (2018).

5.   Persson, N., Algilany, G., Kjellin, D., Ekström, P. & Lilhök, S. *Ageing Management Swedish National Assessment Report*. (2017).

6.   International Atomic Energy Agency. *Safety Aspects of Nuclear Power Plant Ageing*. (1990).

7.   Hart, G. H. A short history of the sump clogging issue and analysis of the problem. *Nucl. News* **47**, 24–34 (2004).

8.   OECD. *NEA/CSNI/R(94)14: Proceedings on the OECD/NEA Workshop in the Barseback Strainer Incident*. (1994).

9.   Rao, D. V, Shaffer, C. J., Leonard, M. T. & Ross, K. W. *NUREG/CR-6808: Knowledge Base for the Effect of Debris on Pressurized Water Reactor Emergency Core Cooling Sump Performance*. (2003).

10.   Nuclear Energy Agency. *Knowledge Base for Strainer Clogging - Modifications performed in different countries since 1992*. (2002).

11.   Zigler, G. *et al. NUREG/CR-6224: Parametric Study of the Potential for BWR ECCS Strainer Blockage Due to LOCA Generated Debris*. (1995).

12.   Rao, D. V. & Souto, F. J. *NUREG/CR-6367: Experimental Study of Head Loss and Filtration for LOCA Debris*. (1996).

13.   *Handbook of Filter Media*. (Elsevier, 2002). doi:10.1016/B978-1-85617-375-9.X5000-7

14.   Ding, M. *et al. NUREG/CR-6877: Characterization and Head-Loss Testing of Latent Debris from Pressurized-Water-Reactor Containment Buildings*. (2005).

15.   Suh, J. K. Evaluation of Long Term Core Cooling Capability Considering LOCA-generated Debris. (Seoul National University, 2015).

16.   Suh, J. K. *et al.* Experimental study of pressure drops through LOCA-generated debris deposited on a fuel assembly. *Nucl. Eng. Des.* **289**, 49–59 (2015).

17.   Lane, A. E. *et al. WCAP-16530: Evaluation of Post-Accident Chemical Effects in Containment Sump Fluids to Support GSI-191*. (2008).

18.   Institute Nuclear Energy. *Pressurized Water Reactor Sump Performance Evaluation Methodolgy*. (2004).

19.   Ali, A. & Blandford, E. D. An Experimental Study on Head Loss of Prototypical

Fibrous Debris Beds During Loss-of-Coolant Accident Conditions. *J. Nucl. Eng. Radiat. Sci.* **2**, 031006 (2016).

20. Williams, C. Drag and Shape Analysis of Fiberglass Particles. (The University of New Mexico, 2016).

21. Parker, J. D. *The Sheet-Forming Process*. (The Technicl Association of the Pulp and Paper Industry, 1972).

22. Kubát, J. & Steenberg, B. Theory of Screening III: Screening at Low Particle Concentrations. *Sven. Papperstidning* **58**, 319–324 (1955).

23. Kubát, J. Theory of Screening VII: Experimental Evidence of the Validity of the Statistical Screening Theory. *Sven. Papperstidning* **59**, 251–256 (1956).

24. Kubát, J. Theory of Screening VI: Screening Processes Involving Particle Interaction. *Sven. Papperstidning* **59**, 175–178 (1956).

25. Andersson, O. & Bartok, W. Application of Feed-back to Fibre Classification. *Sven. Papperstidning* **58**, 367–373 (1995).

26. Radvan, B. & Dodson, C. Detection and Cause of the Layered Structure of Paper. in *3rd Pulp and Paper Fundamental Research Symposium* 189–214 (1965).

27. Lucisano, M. & Norman, B. The forming and properties of quasi-random lab- oratory paper sheets. in *Proceedings from the 1994 International Paper Physics Conference* (1994).

28. Danby, R. The impact of forming fabric structures on print quality. *Pulp Pap. Canada* **95**, 48–51 (1994).

29. Serles, A. & Green, S. Forming fabric weave-scale variations in paper filler content. *Tappi J.* **12**, 9–18 (2013).

30. Mason, S. G. The Motion of Fibres in Flowing Liquids. *Pulp Pap. Mag. Canada* **51**, 93–100 (1950).

31. Kerekes, R. J. & Schell, C. J. Characterization of Fibre Flocculation Regimes by a Crowding Factor. *J. Pulp Pap. Sci.* **18**, 32–38 (1992).

32. Estridge, R. The Initial Retention of Fibers by Wire Grids. (Lawrence College, 1961).

33. Abrams, R. W. The Retention of Fibers from Dilute Suspensions. (Lawrence College, 1964).

34. Jeffery, G. B. The Motion of Ellipsoidal Particles Immersed in a Viscous Fluid. *Proc. R. Soc. A Math. Phys. Eng. Sci.* **102**, 161–179 (1922).

35. Kvick, M. Transitional and turbulent fibre suspension flows. (KTH Royal Institute of Technology, 2014).

36. Håkansson, K. Orientation of elongated, macro and nano-sized particles in macroscopic flows. (KTH Royal Institute of Technology, 2014).

37. Bellani, G. Experimental studies of complex flows through image-based techniques. (KTH Royal Institute of Technology, 2011).

38. Rosén, T. Angular dynamics of non-spherical particles in linear flows related to production of biobased materials. (KTH Royal Institute of Technology, 2016).

39. Håkansson, K. M. O., Lundell, F., Prahl-Wittberg, L. & Söderberg, L. D. Nanofibril Alignment in Flow Focusing: Measurements and Calculations. *J. Phys. Chem. B* **120**, 6674–6686 (2016).

40. Peng, H. PIV Measurements of Flow Through Forming Fabrics. (The University of British Columbia, 2011).

41. Singh, F. Micro-PIV Measurement of Flow Through Forming Fabrics. (The University of British Columbia, 2013).

42. Bellani, G., Lundell, F. & Söderberg, L. D. Experimental Study of Filtration of Fiber Suspensions. Part I: Time-Resolved Measurements of the Formation of a Fiber Network. in *16th Pulp and Paper Fundamental Research Symposium* 255–280 (2017).

43. Redlinger-Pohn, J. D., König, J. & Radl, S. Length-selective separation of cellulose fibres by hydrodynamic fractionation. *Chem. Eng. Res. Des.* **126**, (2017).

44. Eßl, M. Design of a Distributor for Fibre Suspensions. (Graz University of Technology, 2017).

45. Kumar, A. Passage of Fibres Through Screen Apertures. (The University of British Columbia, 1991).

46. Olson, J. A. The effect of Fibre length on passage through narrow apertures. (The University of British Columbia, 1996).

47. Salem, H. J. Modelling the Maximum Capacity of a Pulp Pressure Screen. (The University of British Columbia, 2013).

48. Kerekes, R. J. & Schell, C. J. Effects of fiber length and coarseness on pulp flocculation. *TAPPI J.* **78**, 133–139 (1995).

49. Kim, K.-T. Evolutionary developments of advanced PWR nuclear fuels and cladding materials. *Nucl. Eng. Des.* **263**, 59–69 (2013).

50. Lindström, S. B. & Uesaka, T. Particle-level simulation of forming of the fiber network in papermaking. *Int. J. Eng. Sci.* **46**, 858–876 (2008).

51. Bhatti, H. A. *et al.* Sensitivity study LOCA-generated Debris on the Pressure Drop of Fuel Assembly. in *25th International Conference on Nuclear Engineering* 5 (2017).

52. Lindström, S. B. & Uesaka, T. Particle-level simulation of forming of the fiber network in papermaking. *Int. J. Eng. Sci.* **46**, 858–876 (2008).

53. Andrić, J., Lindström, S. B., Sasic, S. & Nilsson, H. Rheological properties of dilute suspensions of rigid and flexible fibers. *J. Nonnewton. Fluid Mech.* **212**, 36–46 (2014).

54. Lindström, S. B. & Uesaka, T. Simulation of the motion of flexible fibers in viscous fluid flow. *Phys. Fluids* **19**, 113307 (2007).

55. Schmid, C. F., Switzer, L. H. & Klingenberg, D. J. Simulations of fiber flocculation: Effects of fiber properties and interfiber friction. *J. Rheol. (N. Y. N. Y).* **44**, 781–809 (2000).

56. Schmid, C. F. & Klingenberg, D. J. Mechanical Flocculation in Flowing Fiber Suspensions. *Phys. Rev. Lett.* **84**, 290–293 (2000).

57. Redlinger-Pohn, J. D., König, L. M., Kloss, C., Goniva, C. & Radl, S. Modeling of non-spherical, elongated particles for industrial suspension flow simulation. in *ECCOMAS Congress 2016 - Proceedings of the 7th European Congress on Computational Methods in Applied Sciences and Engineering* **1**, (2016).

58. *VDI Heat Atlas*. (Springer Berlin Heidelberg, 2010). doi:10.1007/978-3-540-77877-6

59. Stieß, M. *Mechanische Verfahrenstechnik 1*. (Springer Berlin Heidelberg, 1995). doi:10.1007/978-3-662-08600-1

60. Derakhshandeh, B., Kerekes, R. J., Hatzikiriakos, S. G. & Bennington, C. P. J. Rheology of pulp fibre suspensions: A critical review. *Chem. Eng. Sci.* **66**, 3460–3470 (2011).

61. Lee, S., Hassan, Y. A., Abdulsattar, S. S. & Vaghetto, R. Experimental study of head loss through an LOCA-generated fibrous debris bed deposited on a sump strainer for Generic Safety Issue 191. *Prog. Nucl. Energy* **74**, 166–175 (2014).

62. Lee, S., Abdulsattar, S. S., Vaghetto, R. & Hassan, Y. A. Permeability and compression of fibrous porous media generated from dilute suspensions of fiberglass debris during a loss of coolant accident. *Nucl. Eng. Des.* **291**, 244–260 (2015).

63. Abdulsattar, S. S. Head Loss Through Fibrous Debris Bed with Different Types of Perforated Strainers. (Texas A&M University, 2014).

64. Ali, A. F. & Blandford, E. D. Conventional and chemical head loss modeling of Multi-Constituent debris beds in resolution of GSI-191. in *16th International Topical Meeting on Nuclear Reactor Thermal Hydraulics* 5303–5316 (2015).

65. Ghosh, A. K. *et al.* Accumulation and Head-Loss Characteristics of Selected Pressurized Water Reactor LOCA-Generated Debris. *Nucl. Technol.* **154**, 69–84 (2006).

66. Ghosh, A. K., Howe, K. J., Maji, A. K., Letellier, B. C. & Jones, R. C. Head Loss Characteristics of a Fibrous Bed in a PWR Chemical Environment. *Nucl. Technol.* **157**, 196–207 (2007).

67. Park, J. H., Kasza, K., Fisher, B. & Oras, J. *NUREG/CR-6913: Chemical Effects Head-Loss Research in Support of Generic Safety Issue 191*. (2006).

68. Jung, M.-S. & Kim, K.-T. Debris filtering efficiency and its effect on long term cooling capability. *Nucl. Eng. Des.* **261**, 1–9 (2013).

69. Park, J.-K., Lee, S.-K. & Kim, J.-H. Development of an evaluation method for nuclear fuel debris–filtering performance. *Nucl. Eng. Technol.* **50**, 738–744 (2018).

70. KIM, K.-T., JANG, Y.-K. & KIM, J.-I. In-Reactor Performance of an Advanced PWR Fuel, PLUS7, for OPR1000s in Korea. *J. Nucl. Sci. Technol.* **45**, 836–849 (2008).

9. Appendices

Appendix A: Discussion on Fibre Length, Pool Concentration and Academic Studies Documented in Literature

Studies on fibrous debris prepared from NUKON® glass fibre-based insulation from PCI Performance Contracting, Inc. (USA) is found throughout the literature. The insulation material is mechanically degraded leading to single fibres, and fibre clump breakages. In the NUREG/CR-6224 report, Zigler *et al.* [11] report difficulties in measuring the size and size distribution of fibrous debris generated from NUKON® insulation material. Instead, a classification based on the debris sedimentation velocity was chosen (Table 1). Class 1, and class 2 debris, which are stiff and flexible fibres, are those with a sedimentation velocity of 1 mm/s to 3.5 mm/s. A length span of 5 mm to 25.4 mm was attributed to these classes. In Figure 23a we show the length dependent sedimentation velocity for cylindrical fibres parallel to the flow direction (drawn as a dashed line), and normal to the flow direction (drawn as a dash-dotted line). For that we solve the force balance equation settling prolate spheroids, documented for example in Redlinger-Pohn *et al.* [57]. The diameter is set to the value for glass fibres from NUKON® insulation, which is ca. 7 μm (PCI Performance Contracting, Inc., USA). Pool temperature and thus fluid properties of the suspending water varies with time. We therefore calculated the sedimentation velocity in dependence on the fibre length for temperatures of 20°C, and 80°C with fluid properties taken from the VDI Heat Atlas for water[58] and glass fibre density taken as temperature independent and equal to 2500 kg/m³. The fibre length and sedimentation velocity stated in the literature correspond to a water temperature of 80°. The upper sedimentation velocity for a fibre aligned in flow direction however levels off at ca. 2 mm/s, which is lower than the maximum sedimentation velocity reported in literature. This raises questions whether particle interaction where at hand in the sedimentation test. Hence, the reported sedimentation velocity probably does not represent a particle property that is related to its size, but a property of several particles acting together. The fibre-lengths reported by Suh [15] are marked with an orange shadow in Figure 23a.

A length distribution adapted from Suh [15] is presented in Figure 23b. The fibre-length distribution was measured with an L&W Fibre Tester Plus, which is a standard measurement for the characterisation of cellulose fibre pulp. The results were reported as fractions and converted into a cumulative distribution. Unfortunately, Suh [15] failed to report the basis of the distribution, i.e. number of fibres or total length. Both scenarios are presented in Figure 23b. The solid line is based on the assumption that the fibre length distribution is reported based on the cumulative length. Mean length-based fibre length L_1 is then calculated to 0.73 mm and 0.57 mm, for the APR1400 and WCAP preparation methods, respectively. The corresponding x_{90} length, that is the length exceeded by 10% of the fibre population, is 1.56 mm and 1.16 mm for the APR1400 and WCAP preparation methods, respectively. The dashed line is based on the assumption that the fibre length distribution is reported on the basis of the cumulative number of fibres with a certain length. The data were converted from number-based distribution to length-based distribution. Detailed explanations on the handling of particle size distribution are found in standard books in particle engineering,

for example Stieß [59]. The corresponding length for APR1400 and WCAP were then: L_1 1.25 mm and x_{90} 2.34 mm, and L_1 1.02 mm and x_{90} 2.13 mm.
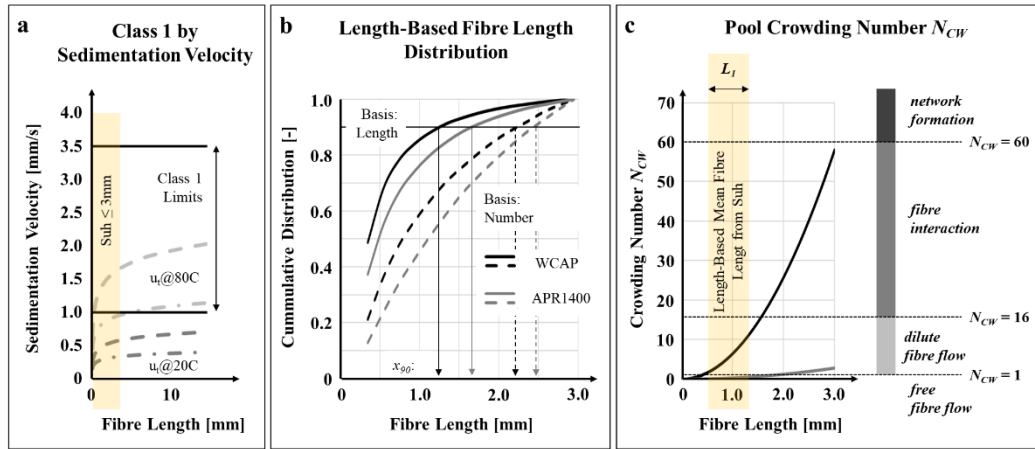
Figure 23: Length of fibres in Nuclear Power Plant and resulting networking regime. a: fibre length following sedimentation velocity reported for class 1 NUKON® insulation debris [11]. b: Fibre-length distribution from Suh [15] plotted as cumulative length distribution. Solid line: assumption that the original distribution basis is length. Dashed line: assumption that the original distribution basis is number. c: Crowding number NCW for given fibre pool concentration depending on the fibre length. According to fibre network regimes are stated on the right side. Orange highlighted area corresponds to the fibre length reported by Suh [15].

The significance of the length-averaged fibre length L_1 is found from its description of the state of fibre crowding. Following the definition of the Crowding number in equation (1), L_{Fibre} is the length-averaged mean fibre length L_1. Crowding numbers that can be expected in the pool as a function of fibre length is presented in Figure 23c. The black, and grey solid line denote results for the upper and lower limits on the fibre concentration after LOCA reported by Zigler *et al.* [11] as 0.047vol%, and 0.002vol%, respectively. These concentrations were calculated from breakage scenarios that result in 0.79 m³ of fibres in 1668 m³ of water, and 0.04 m³ of fibre in 1741 m³ of water. To the right of the length dependent crowding number, the suspension regime classification as reported by Kerekes and Schell [31] and in the review of Derakhshandeh *et al.* [60] is provided. For a crowding number $N_{CW} < 1$, fibres are nearly undisturbed by each other and free flowing. For a crowding number $1 < N_{CW} < 16$, fibres are interacting, but the number of permanent fibre-fibre contacts is too small to form networks. Network effects need to be accounted for only at higher crowding numbers. In this context, the assumption of a full dispersion of the dislocated fibres is a conservative one and leads to an upper limit of the computed N_{CW}. In case fragments of the insulation material remain non-fibrillated, those flakes will be retained by the strainer (Filtration efficiency for class 3 and higher particles is reported as 1, Table 1). If some fibres are bound in flakes, the concentration of free fibres that may network as a result of suspension flow is lower, and thus N_{CW} is lower. Upper and lower N_{CW} that results from the fibre concentration reported by Zigler *et al.* [11], and fibre length reported by Suh [15] are 10 and 0.1, respectively for LOCA generated fibres. The number, or volume, of latent fibres is even smaller [7]. We can thus conclude that a free fibre flow to dilute fibre flow can be expected in NPP. The length of the larger fibres, which retention is expected to be higher than for smaller fibres, is 1.16 mm or 2.34 mm depending on the basis of the data. Relating to the discussion in the chapter *Formation of Fibre Mat on Meshes in Paper Production*, fibre filtration versus suspension thickening, it can be argued that fibre filtration is to be expected.

Strainer and Screens

On LOCA related filtration tests Rao *et al.* [9] note horizontal and vertical laboratory scale tests, as well as tests on larger prototypical and semi-industrial scale strainers. The first two are usually found in academic tests, with a high proportion of the horizontal test in a flow loop configuration. An overview of selected literature work on head-loss tests on strainers and screens are given in Table 6. An important note is made by Rao *et al.*, namely the difference in typical screen design between BWR and PWR. BWR strainers are typically perforated plates (or hole plates), and PWR screens are typically wire meshes (the majority seems to have a mesh size of 3.175 mm).

Table 6: Test facilities documented in the literature. Screen geometry defined by D_{Open}, and S_{Open}. Approach velocity u_n of the fibre suspension. Hor. is a horizontal approach direction and Ver. a vertical approach direction.

Description	Prep. Method	Filtration Set-Up	Screen	Approach Velocity [mm/s]
Lee *et al.* [61,62], and Abdulsattar [63] performed experiments to extend the NUREG pressure loss model [11] to larger mat thickness.	NEI	Vert.	Staggered hole plate	3
			D_{Hole} 2.42 mm	12
			S_{Hole} 3.96 mm	31
Ali and Blandford [19,64] performed chemical head loss tests to present their modified NEI preparation method.	Mod. NEI	Hor.	Hole plate:	Not stated
			D_{Hole} 2.39 mm	
			S_{Hole} not stated	
Gosch *et al.* [65,66] compared pressure loss from NUKON® and CalSil insulation material. CalSil formed smaller fragments that alone did not cover the screen.	Shredded	Hor.	Wire mesh	150
			D_{Hole} 3.2 mm	270
			S_{Hole} not stated	
Rao *et al.* [12] quantified the pressure loss across a debris field filtering particle for comparison to numerical models. Screen resembled BWR suction strainer.	Leaf shredder	Hor.	Staggered hole plate	46
			D_{Hole} 3.18 mm	457
			S_{Hole} ca. 1.59 mm	
Park *et al.* [67] performed filtration tests to quantify the chemical effect, i.e. particular precipitates, on the pressure loss. NULON® fibre glass shreds are reported as 1 cm to 2 cm breaks.	Leaf shredder	Hor.	Staggered hole plates	30
			D_{Hole} 4.76 mm	
			S_{Hole} 1.59 mm	
			D_{Hole} 3.18 mm	
			S_{Hole} 1.58 mm	

Appendix B: Design of Fuel Assembly Protection Layer

Summary of the Literature Survey

Fuel assembly grids (i) hold the fuel rods in position, (ii) introduce fluid mixing to enhance heat transfer from the fuel rods, and (iii) protect the fuel rods from harmful suspended materials, i.e. metal threads [49,68–70]. However, fibres are found to accumulate on the fuel assembly. In particular, that is documented on studies on the PLUS7 protective grid fuel assembly used in (Korean) PWR [15,16,51]. The formed fibre mat has the capability to filter particles and this leads to an increase in pressure loss and consequently a reduction in flow rate through the protective layer.

Fuel production, and fuel assembly design are scarcely documented in the open literature. Only a few publications hint on the design values, and they will be reviewed following. Those are the basis for the 3D reproduction of the PLUS7 fuel assembly used in this study.

Protective grids are placed after the inlet nozzle in the fuel chamber to filter metal debris, for example, metal threads which are lost during metal work, from the fluid. Their design development is reviewed by Kyu-Tae Kim [49], Figure 24. The driver of the development was to improve the retention of metal parts from the coolant flowing into the fuel assembly, which causes wear on the fuel. The aim is a spacer grid design which results in zero fretting wear-induced fuel failure and good fluid mixture to facilitate the heat transfer.

Jung and Kim [68] give a good description of three types of protective grids that are employed in PWR: *SYS80*, *Guardian*, and *PLUS7*. The publication lists geometrical details on the fuel assembly, which became the basis for our 3D printed reproduction used in fibre retention tests. The main difference is the shape and size of their openings, as well as additional layers of protection. They investigated the retention of debris with the smallest dimension of 5 mm by 2.5 mm by 2 mm, and the largest dimension of diameter 2.6 mm and length of 36 mm. A hole plate screen alone retained 26% (equivalent to SYS80 protective grid), whilst PLUS7 (P-grid), and Guardian (G-grid) are enhanced by a structured grid placed on-top could filter 91%, and 96% respectively. Retention of LOCA debris is discussed based on geometrical aspects. Fibre mat formation is not mentioned.

Joon-Kyoo Park *et al.* [69] compared PLUS7, and 17ACE7 fuel assembly in the same spirit. Debris were spheres with diameters ranging from 2 mm to 5 mm, and needles with diameters ranging from 1 mm to 2.5 mm and lengths ranging from 10 mm to 50 mm. Both designs had a comparable filter capability. Up to 50% of the debris were retained at the nozzle, and 25% at the protective grid. The rest was found at the bottom and mid-grid (spacers).

Jeong Kwan Suh [15] discussed the retention and deposition of fibres in a PLUS7 fuel assembly. The number of fibres was based on non-fibrous insulation, but the presence of latent fibres. Those were modelled by NUKON® fibres whose preparation followed the WCAP-16793 method and the APR1400 method. The APR1400 method resulted in slightly longer fibre fragments (see the discussion in Appendix A, and Figure 23). Presence of debris from coatings, chemical precipitates, and latent particles were considered. Chemical precipitates were expressed by AlOOH only. The precipitate was prepared according to WCAP-16530-NP: from aluminium nitrate and sodium hydroxide. The test procedure was (1) addition of

particulate debris, (2) addition of fibres in one or several batches, and (3) addition of chemical precipitates in one or several batches. The pressure loss of fibres and debris was small, compared to the sharp increase with the introduction of chemical precipitates. The pressure drop occurred over the first PLUS7 protective grid layer. The pressure loss over the following layers was negligible. The pressure loss in all cases was below the available pump pressure budget. A significant difference was found with respect to the fibre length: the longer fibres (after APR1400) were all retained at the PLUS7 BN/P-grid. The pressure loss reached a high plateau level (ca. 19 kPa). The shorter fibres (after WCAP-16793) deposited on the first PLUS7 BN/P-grid. Pressure loss spiked with the addition of chemical precipitates and settled on a lower plateau level (ca. 5 kPa). Fibres were found downstream of the first layer. These results represent the importance in the understanding of the fibre properties, especially the aspect ratio, length as well as length distribution, and concentration.
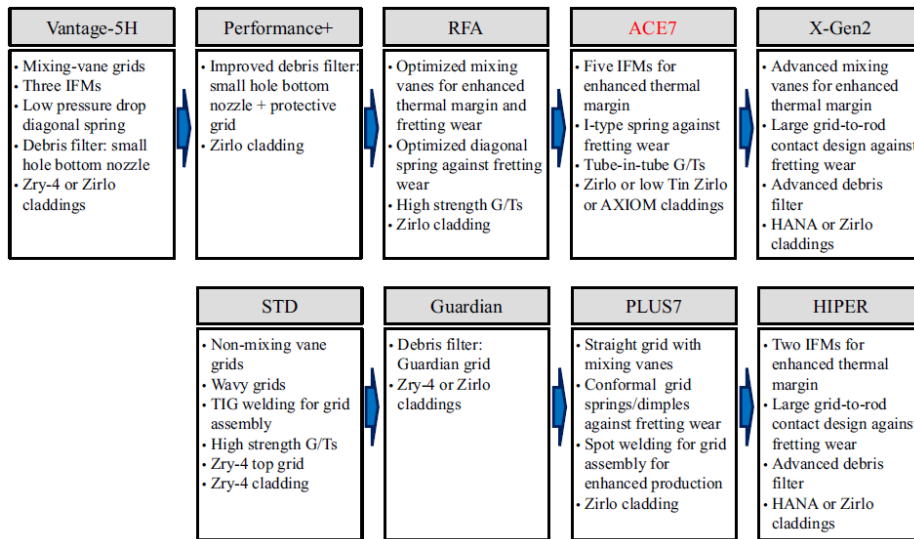
Figure 24: Evolutionary changes in design features of advanced PWR fuels. Reproduced from Kyu-Tae Kim [49].

Hammad Aslam Bhatti *et al.* [51] performed studies in the spirit of Suh [15]. The retention and pressure drop of LOCA suspension containing fibres and precipitates were studied. Glass fibre and fibres from fibre wool were tested. The added mass was the same. Data on the fibres are not reported beside a statement that the fibre wool is finer and/or has lower bulk density. Chemical precipitates were modelled by a mixture of sodium silicate and aluminium nitrate, which formed sticky precipitates. The pressure drop with glass fibre was ca. 30 kPa and did not change with the addition of chemical precipitates. The pressure drop of fibre wool was ca. 45 kPa, spiked to 60 kPa when chemical precipitates where added and dropped back thereafter.

Protective Grid Design

Models of the PLUS7 protective grid and SYS80 protective grid, which is the base layer of Guardian protective grid were reproduced by means of additive manufacturing (3D printing). The material thickness of PLUS7 grid layer 2, and 3 was enhanced to allow production. The grids had been produced by material extrusion type additive manufacturing inhouse (in the Fluid Physics Laboratory, KTH Mechanics), and external (Prototype Lab, KTH, Stockholm). Both gave a good result, where the external printed grid showed a better

resolution, i.e. smoother surface. Key parameters with material extrusion additive manu-facturing are the nozzle speed, and temperature of the nozzle, and base layer. First fibre retention tests were performed with a PLUS7 grid layer 1. Results are documented in the chapter *Fibre Mat Formation on Fuel Assemblies*. Design specifications are taken from Table 1, Figure 5, and Figure 6 from the paper of Jung, and Kim [68], here Table 7, Figure 25, and Figure 26.

Table 7: Reproduction of Table 1 in Jung, and Kim [68]. Important design parameters in the reproduction are highlighted.

Design parameter	PLUS7	Guardian	SYS80
Region application year	2006	2001	1994
Fuel rod diameter (mm)	9.50	9.70	9.70
Fuel rod pitch (mm)	12.85	12.85	12.85
Fuel assembly pitch (mm)	207.77	207.77	207.77
Debris filter grid	P-grid	G-Grid	–
Inner strap height (mm)	19.81	38.30	–
Inner strap thickness (mm)	0.267	0.457	–
Number of debris filter dimples per unit cell	4	4	–
Number of retention springs per unit cell	–	2	–
Number of rod supporting dimples per unit cell	–	4	–
Bottom nozzle			
Circular flow-hole (mm)	4.95	10.72	10.72
Slot flow-hole (mm)	4.95 × 7.44	–	–

Protective Grid PLUS7

Figure 25 presents key dimensions of the protective grid layer 1 (inlet plate), layer 2 (thin plates), and layer 3 (thin plate with dimples which connect to the fuel rod). Quantities in grey are extracted from the drawings and/or from the description in Table 7.
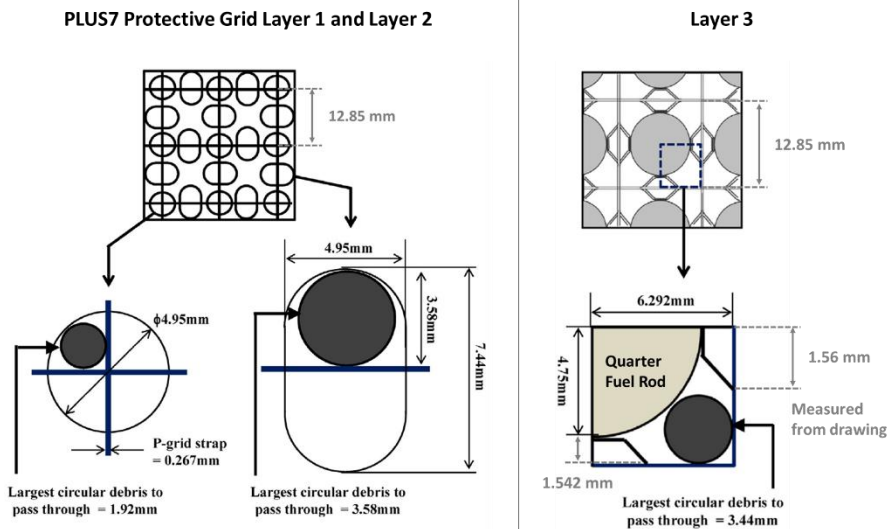
Figure 25: Key dimension of PLUS7 protective grid. Adapted from Jung, and Kim, [68], Fig. 6. Quantities in grey are measured from the figure and added to the sketch.
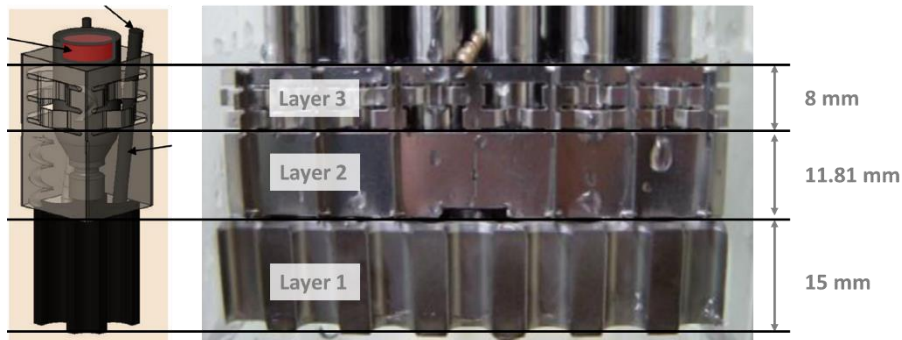
PLUS7 Protective Grid

Layer 3 — 8 mm
Layer 2 — 11.81 mm
Layer 1 — 15 mm

Figure 26: Drawing and experiment set-up snapshots from Jung and Kim [68]. Adapted with modifications from paper Fig. 9, and Fig. 5.

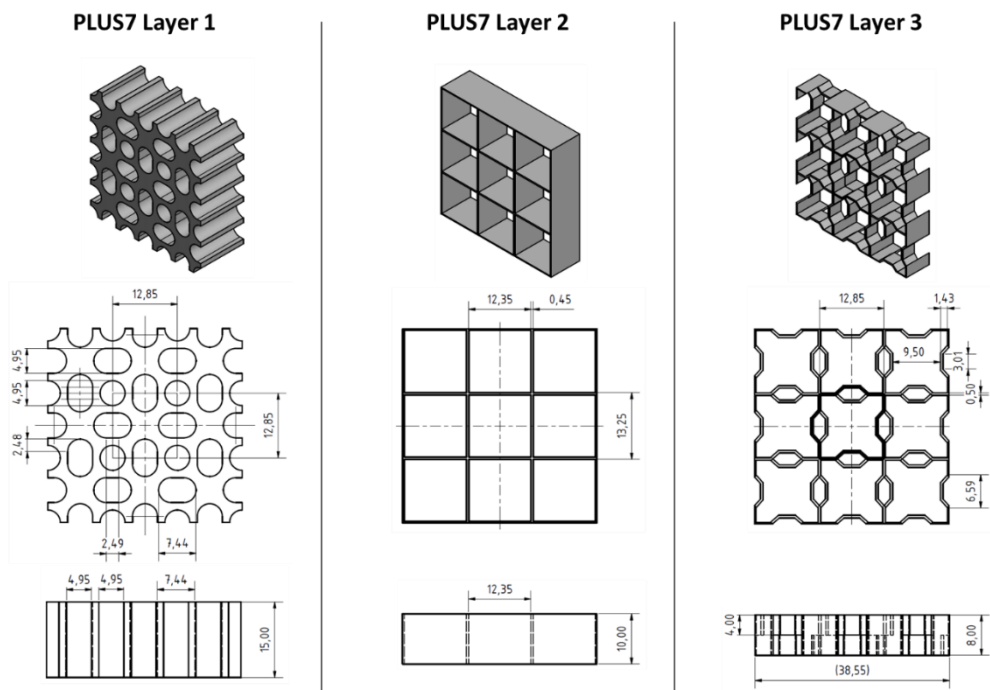PLUS7 Layer 1 — PLUS7 Layer 2 — PLUS7 Layer 3

Figure 27: Sketches of the PLUS7 protective grid. A section of 9 by 9 fuel rods is displayed which has outer dimensions of 38.55 mm by 38.55 mm.

The height of the different layers is not specified. It is assumed, that the parameter *inner strap height* refers to the height of the protective layer excluding the inlet plate, layer 1. In the case of the PLUS7 protective grid, the height is of layer 2 and layer 3 is guessed from paper Fig. 5, shown in Figure 26. Layer 2 is ca. 3/5 of the height, ca. 11.81 mm, and layer 3 is 2/5 of the height, ca. 8 mm. The height of layer 1 is assumed to be 15 mm. The thickness of the *P-grid-strap* is increased to 0.45 mm, to allow 3D printing with extruded filaments (resolution problems). A section of the final shop drawing of PLUS7 protective grid is shown in Figure 27. The 3D printed PLUS7 protective grid layers 1 to 3 are shown in Figure 28.
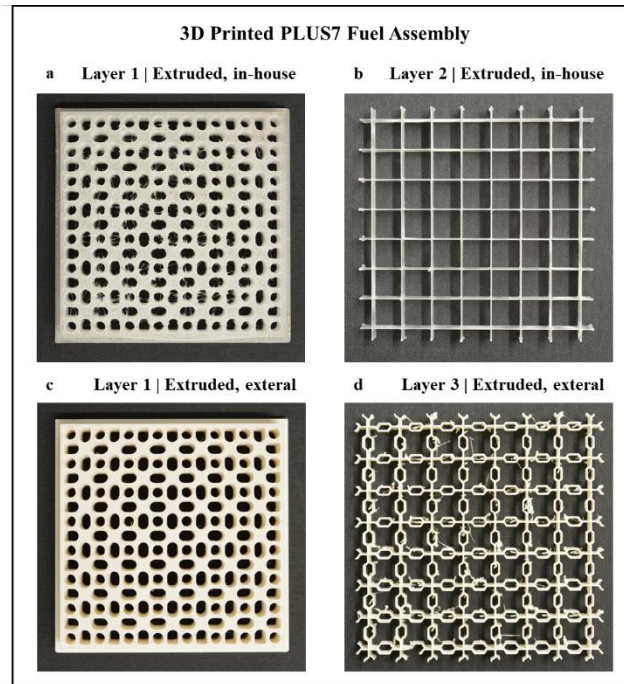
Figure 28: 3D printed PLUS7 protective grid layer. a, and b: printed in-house. c and d: printed external at KTH prototyping lab.

Protective Grid Guardian and SYS80

The protective grid Guardian builds on a first layer which is equivalent to the SYS80 protective grid. Figure 29, and Figure 30 present the literature basis for the design of SYS80, and the Guardian protective grid layer. Figure 31 presents the 3D printed SYS80 or Guardian Layer 0 protective grid. The main differences in the geometry to the PLUS7 Layer 1 are the hole size and hole spacing.
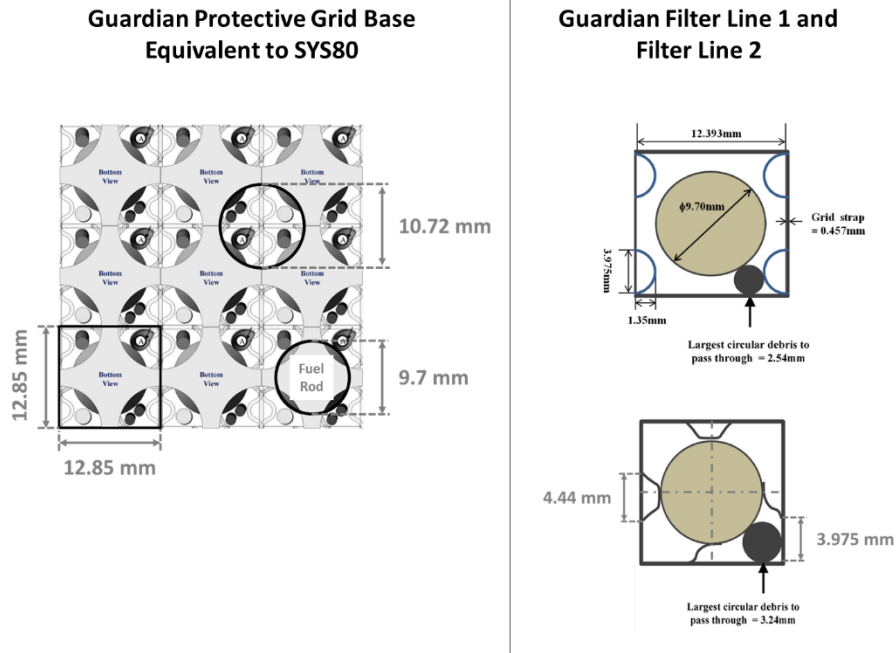
Figure 29: Key dimension of the PLUS7 protective grid copied and modified from Jung, and Kim [68]. Quantities in grey are added to the sketch.

Guardian Protective Grid
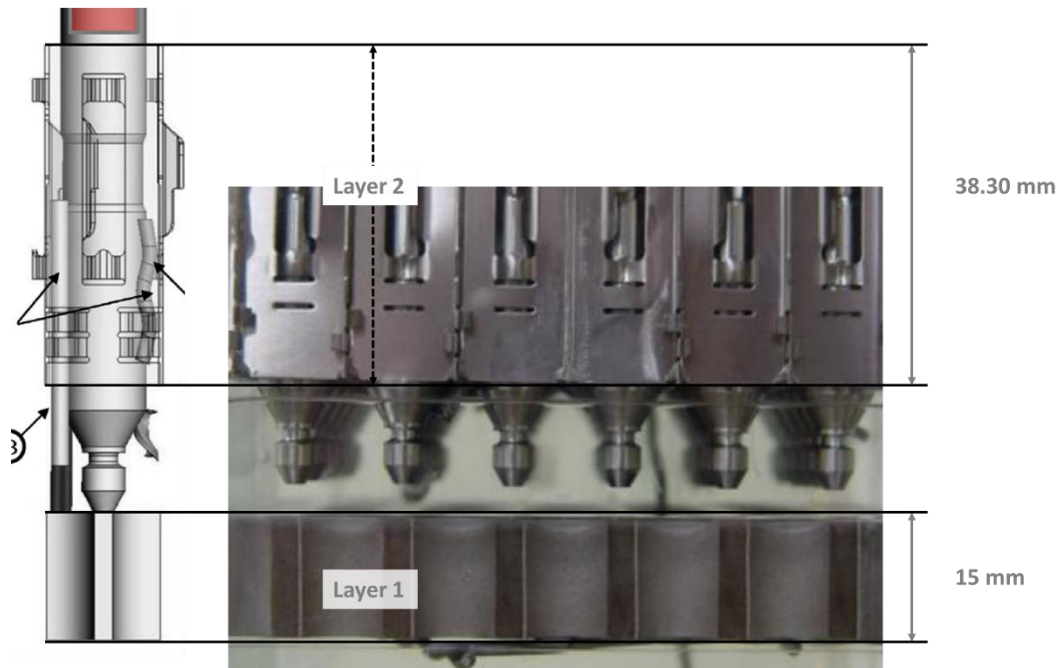
Figure 30: Drawing and experiment set-up snap shots from Jung and Kim.
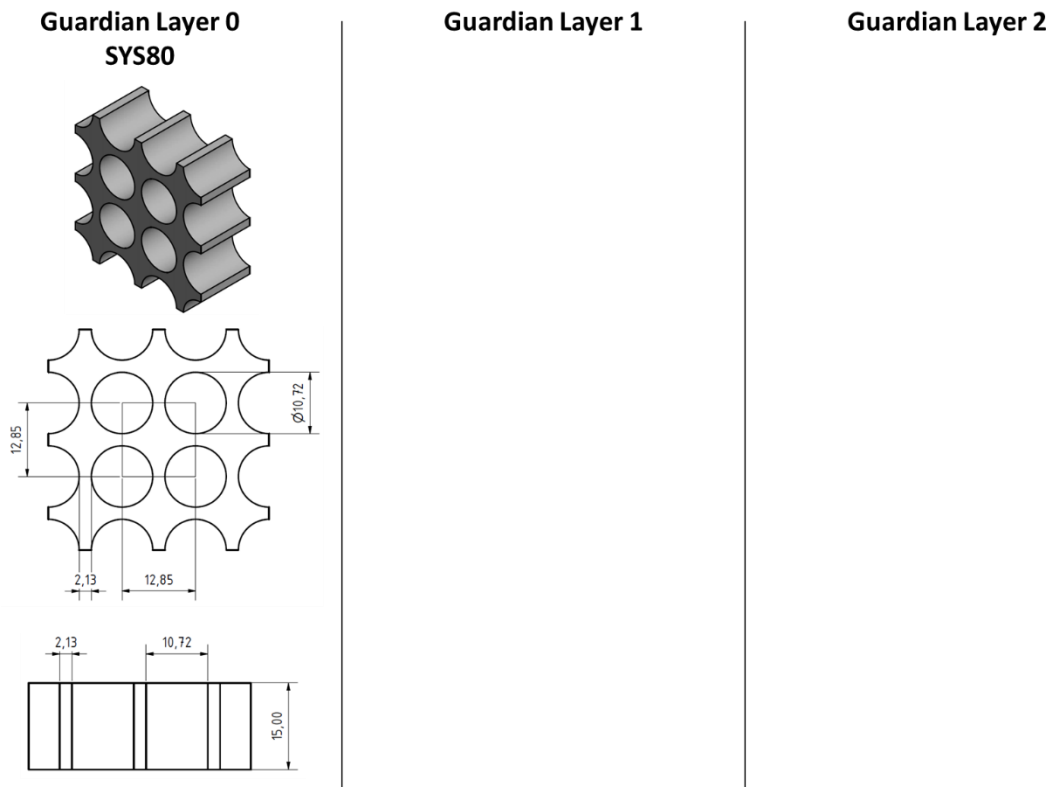

Figure 31: Sketches of the Guardian protective grid. A section of 9 by 9 fuel rods is displayed which has outer dimensions of 38.55 mm by 38.55 mm. Guardian Layer 0 is equivalent to SYS80. Drawings of Guardian Layer 1. Layer 2 has not been completed.

The Swedish Radiation Safety Authority has a comprehensive responsibility to ensure that society is safe from the effects of radiation. The Authority works from the effects of radiation. The Authority works to achieve radiation safety in a number of areas: nuclear power, medical care as well as commercial products and services. The Authority also works to achieve protection from natural radiation an to increase the level of ratiation safety internationally.

The Swedish Radiation Safety Authority works proactively and presentively to protect people and the environment from the harmful effects of radiation, now and in the future. The Authority issues regulations and supervises compliance, while also supporting research, providing training and information, and issuing advice. Often, activities involving radiation require licences issued by the Authority. The Swedish Radiation Safety Authority maintains emergency preparedness around the clock with the aim of limiting the aftermath of radiation accidents and the unintentional spreading of radioactive substances. The Authority participates in international co-operation in order to promote radiation safety and finances projects aiming to raise the level of radiation safety in certain Eastern European countries.

The Authority reports to the Ministry of the Environment and has around 300 employees with competencies in the fields of engineering, natural and behavioral sciences, law, economics and communications. We have recieved quality, environmental and working environment certification.